International Journal of Nanomedicine

Dovepress
open access to scientific and medical research

Open Access Full Text Article

ORIGINAL RESEARCH

Evaluation of Anticancer Efficacy of D-α-Tocopheryl Polyethylene-Glycol Succinate and Soluplus® Mixed Micelles Loaded with Olaparib and Rapamycin Against Ovarian Cancer

Yu Been Shin[1]*, Ju-Yeon Choi[2]*, Moon Sup Yoon[1], Myeong Kyun Yoo[1], Dae Hwan Shin[1,3]*, Jeong-Won Lee[4,5]*

[1]College of Pharmacy, Chungbuk National University, Cheongju, 28160, Republic of Korea; [2]Research Institute for Future Medicine, Samsung Medical Center, Sungkyunkwan University School of Medicine, Seoul, South Korea; [3]Chungbuk National University Hospital, Chungbuk National University, Cheongju, 28644, Republic of Korea; [4]Department of Obstetrics and Gynecology, Samsung Medical Center, Sungkyunkwan University School of Medicine, Seoul, South Korea; [5]Samsung Advanced Institute for Health Sciences & Technology, Sungkyunkwan University School of Medicine, Seoul, 06351, Republic of Korea

*These authors contributed equally to this work

Correspondence: Dae Hwan Shin, College of Pharmacy, Chungbuk National University, Osongsaengmyeong 1-ro, Osong-eup, Heungdeok-gu, Cheongju, 28160, Republic of Korea, Tel +82 43 261 2820, Fax +82 43 268 2732, Email dshin@chungbuk.ac.kr; Jeong-Won Lee, Department of Obstetrics and Gynecology, Samsung Medical Center, Sungkyunkwan University School of Medicine, 81, Irwon-ro, Gangnam-gu, Seoul, South Korea, Zip 06351, Tel\Fax +82-2-3410-1382, Email garden.lee@samngsung.com

Purpose: Ovarian cancer has the highest mortality rate and lowest survival rate among female reproductive system malignancies. There are treatment options of surgery and chemotherapy, but both are limited. In this study, we developed and evaluated micelles composed of D-α-tocopheryl polyethylene-glycol (PEG) 1000 succinate (TPGS) and Soluplus® (SOL) loaded with olaparib (OLA), a poly(ADP-ribose)polymerase (PARP) inhibitor, and rapamycin (RAPA), a mammalian target of rapamycin (mTOR) inhibitor in ovarian cancer.

Methods: We prepared micelles containing different molar ratios of OLA and RAPA embedded in different weight ratios of TPGS and SOL (OLA/RAPA-TPGS/SOL) were prepared and physicochemical characterized. Furthermore, we performed in vitro cytotoxicity experiments of OLA, RAPA, and OLA/RAPA-TPGS/SOL. In vivo toxicity and antitumor efficacy assays were also performed to assess the efficacy of the mixed micellar system.

Results: OLA/RAPA-TPGS/SOL containing a 4:1 TPGS:SOL weight ratio and a 2:3 OLA:RAPA molar ratio showed synergistic effects and were optimized. The drug encapsulation efficiency of this formulation was >65%, and the physicochemical properties were sustained for 180 days. Moreover, the formulation had a high cell uptake rate and significantly inhibited cell migration (**$p < 0.01$). In the in vivo toxicity test, no toxicity was observed, with the exception of the high dose group. Furthermore, OLA/RAPA-TPGS/SOL markedly inhibited tumor spheroid and tumor growth in vivo.

Conclusion: Compared to the control, OLA/RAPA-TPGS/SOL showed significant tumor inhibition. These findings lay a foundation for the use of TPGS/SOL mixed micelles loaded with OLA and RAPA in the treatment of ovarian cancer.

Keywords: mixed micelle, combination therapy, nanoformulation, IV formula, antitumor efficacy

Introduction

Ovarian cancer, which ranks first in mortality among malignant tumors of the female reproductive system, has the lowest survival rate of all gynecologic malignancies despite advances in diagnosis and treatment.[1,2] Specifically, epithelial ovarian cancer represents about 90% of all malignant ovarian tumors.[3] The prevailing treatment approach for this type of cancer typically involves cytoreductive surgery coupled with chemotherapy based on platinum compounds.[4,5] Although

Received: 14 March 2024
Accepted: 2 July 2024
Published: 2 August 2024

Graphical Abstract

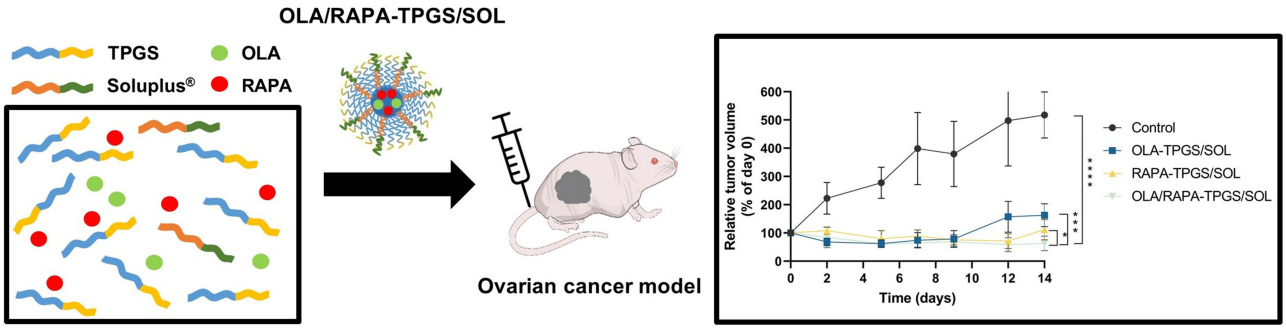

these treatments have good initial responses rates, the recurrence rate is as high as 70%,[6] and chemotherapy is limited by drug resistance[7] and side effects.[8]

Poly(ADP-ribose) polymerase (PARP) inhibitors, which target the PARP protein,[9,10] selectively target tumor cells that are unable to repair DNA double-strand breaks,[11,12] and can enhance neoantigen expression to generate an antitumor immune response.[13,14] Currently, inhibitors targeting PARP have gained approval for use in treating various cancers, including ovarian,[15] breast,[16] and pancreatic,[17] with several clinical trials enrolled. Olaparib (OLA) is a prime example of a PARP inhibitor and was the first monotherapy approved by the FDA for the treatment of BRCA-mutated ovarian cancer.[18] Cells with mutated BRCA function have a homologous recombination (HR) deficiency, which is reported to be present in a significant proportion of non-BRCA-mutated ovarian cancers.[19,20] Despite the high therapeutic efficacy of OLA, its oral bioavailability is low due to its low solubility and permeability.[21,22]

The mammalian target of rapamycin (mTOR), a serine/threonine kinase, orchestrates cellular growth, proliferation, and viability.[23,24] Notably, the mTOR signaling pathway may become excessively active in and lead to tumor development, including ovarian cancer.[25,26] Because rapamycin (RAPA) regulates the translation of mRNA, it delays cell cycle progression and thus inhibits cell proliferation.[27] Therefore, RAPA is considered a potential therapeutic agent to inhibit tumor growth.[28,29] However, like OLA, RAPA, also demonstrates the disadvantages of low solubility and bioavailability.[30]

Using polymeric micelle formations presents a plausible method for augmenting the solubility and stability of hydrophobic medications[31,32] Polymeric micelles exhibit high solubility,[33,34] loading capacity,[35] blood flow stability,[36,37] and therapeutic potential.[38] D-α-tocopheryl polyethylene-glycol (PEG) 1000 succinate (TPGS) is a natural water-soluble derivative of vitamin E,[39,40] and increases drug solubility and bioavailability.[41,42] In addition, it is used as an anticancer agents, as it induces apoptosis and exhibits synergistic effects with other anticancer agent.[43] TPGS exhibits anticancer properties akin to those of α-tocopheryl succinate (TOS), with heightened efficiency in triggering apoptosis and producing reactive oxygen species when compared to TOS.[44] Furthermore, TPGS suppresses heightened P-glycoprotein (P-gp) expression,[45–47] a factor significantly implicated in the emergence of multidrug resistance (MDR) cancerous cells.[48,49] While TPGS offers numerous benefits, it possesses a notably high critical micelle concentration (CMC) of 0.02wt%, which may lead to its dissociation in the bloodstream.[39] Soluplus® (SOL), a polyvinyl caprolactam–polyvinyl acetate–polyethylene glycol graft copolymer (PCL-PVAc-PEG), is an amphipathic copolymer. As an amphiphilic substance, SOL can improve the bioavailability of poorly soluble drugs and can self-assemble into micelles above the CMC.[50] Mixed micelles can decrease CMC values,[51] and increase drug activity while decreasing its cytotoxicity.[52] Moreover, mixed micelles offer benefits such as improved micelle stability and drug encapsulation efficiency.[53,54] Several studies of mixed micellar systems have also achieved clinical-stage research status.[54] Studies on various combinations of TPGS and SOL have also been reported.[55,56]

Tumor spheroids are three-dimensional (3D) structures of cancer cells that closely mimic solid tumors in living organisms, replicating their structural composition and dynamic microenvironment.[57] They facilitate cell-matrix

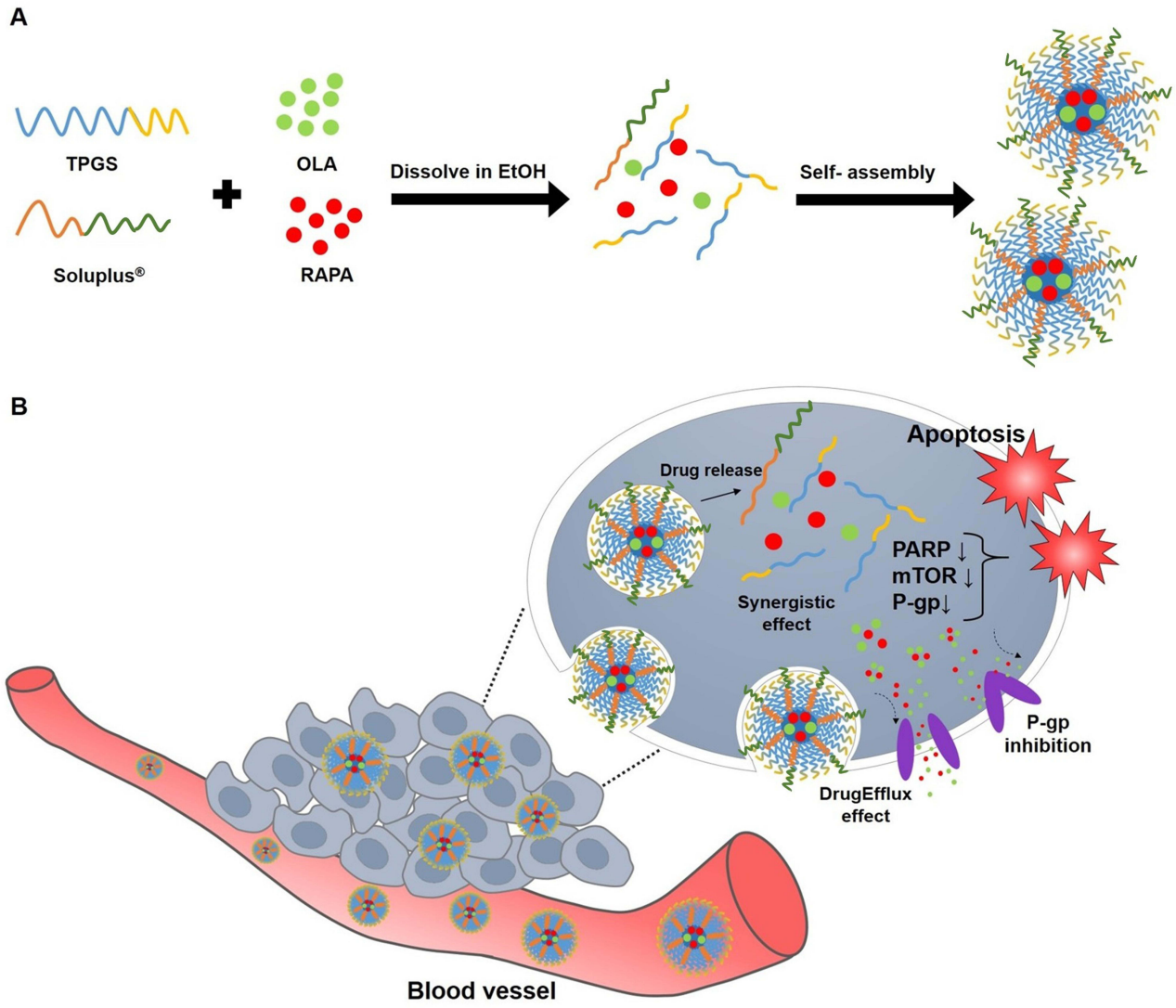

Figure 1 Schematic diagram of (**A**) micelle preparation of TPGS, SOL, OLA, and RAPA and (**B**) representation of the behavior of OLA/RAPA-TPGS/SOL in cancer cells.
Abbreviations: TPGS, D-α-tocopheryl polyethylene-glycol (PEG) 1000 succinate; SOL, Soluplus®; OLA, olaparib; RAPA, rapamycin; EtOH, ethanol; PARP, poly(ADP-ribose) polymerase; mTOR, mammalian target of rapamycin; P-gp, P-glycoprotein; EPR effect, enhanced permeability and retention.

interactions, a feature difficult to achieve in traditional two-dimensional (2D) cell cultures.[58] Additionally, their use reduces the need for animal experimentation, making them an ethical and efficient platform for drug screening and evaluation.[59,60] In this research, we focused on the development and assessment of innovative nanoformulations. These nanoformulations were engineered for enhanced permeability and retention (EPR) by encapsulating a combination of synergistic drugs,[61,62] OLA and RAPA, within mixed micelles. The micelles were formulated using two biocompatible copolymers, namely TPGS and SOL. The unique combination of TPGS, SOL, OLA, and RAPA was investigated for the first time in this study, revealing promising potential as a therapeutic approach for the treatment of ovarian cancer (Figure 1).

Materials and Methods

Materials and Reagents

OLA and RAPA were procured from LC Laboratories® (Woburn, MA, USA). TPGS, coumarin 6 (C6), thiazolyl blue tetrazolium bromide (MTT), *tert*-butanol, triton X-100, sodium hydroxide (NaOH) solution, Cremophor EL® and

dimethyl sulfoxide (DMSO) were procured from Sigma-Aldrich (St. Louis, MO, USA). The SOL was kindly provided by BASF (Ludwigshafen, Rhineland-Palatinate, Germany). Ethanol (EtOH) was procured from Honeywell Burdick & Jackson (Muskegon, MI, USA). Acetonitrile was purchased from Thermo Fisher Scientific (Waltham, MA, USA). Distilled water (DW) of high purity was acquired from Tedia company (Fair-field, OH, USA). All other chemicals and reagents utilized in this study were of analytical reagent grade.

High-Performance Liquid Chromatography Analysis

Quantitative assessment of OLA and RAPA in our samples was executed using a Waters High-performance liquid chromatography (HPLC) system (Milford, MA, USA), which included a 2695 separation module and a 2996 photodiode array detector. A Fortis C18 chromatography column (5 μm, 4.6×250 mm) was utilized, set a temperature of 30°C for the analysis.

The separation of OLA and RAPA was achieved using an isocratic elution method, with each injection comprising 10 μL. The mobile phase was a blend of acetonitrile and DW, mixed in a 70:30 (*v/v*) ratio, and propelled at a flow rate of 1.0 mL/min. OLA detection was conducted at a wavelength of 276 nm with a retention time of approximately 3 min. In the case of RAPA, it was detected 277 nm, having a retention time of 20 min. The quantification of each drug's concentration was accomplished by comparing the peak area to the calibration curve.

Cell Lines and Culture Conditions

Human ovarian cancer HeyA8 cells, were gift from Dr.Anil K. Sood, Department Cancer Biology, University of Texas M.D. Anderson Cancer Center, TX, USA. The cell culture reagents, including penicillin-streptomycin solution, fetal bovine serum (FBS), Roswell Park Memorial Institute 1640 (RPMI 1640) medium, and trypsin, were procured from Corning Inc. (Corning, NY, USA). Dulbecco's phosphate buffered saline (DPBS) was obtained from Biowest (Nuaille, France). The cells were cultured in RPMI 1640 medium, enhanced with a 1% (w/v) concentration of penicillin-streptomycin solution and a 10% (v/v) addition of FBS. Cell culture was performed at 37°C in a 5% CO_2 atmosphere.

Preparation of TPGS and SOL Mixed Micelles and Drug-Loaded Mixed Micelles

Micelles using only TPGS and SOL without drug loading (TPGS/SOL) were prepared using either thin-film hydration or freeze-drying methods, while OLA and RAPA loaded TPGS/SOL micelles (OLA/RAPA-TPGS/SOL) were prepared using thin-film hydration method.

For the thin-film hydration method,[63] the weighed TPGS, SOL, OLA, and RAPA were dissolved in 1 mL of EtOH. This solution was then transferred into a round-bottomed flask and subjected to vacuum evaporation using a rotary evaporator (EYELA®, Bohemia, NY, USA) for 10 min in a water bath set at 40°C. Following the formation of a thin film, 1 mL of DW was introduced and the mixture was hydrated for 30 min to form a homogeneous TPGS/SOL solution.

For the freeze-drying method,[64] TPGS and SOL were weighed at various weight ratios and dissolved in 1 mL of *tert*-butanol at 60°C. Following the addition of 1 mL of 60°C DW, the TPGS/SOL solution was vortexed. The samples were then frozen at −70°C for 1 h and lyophilized at a shelf temperature of −20°C and a condenser temperature of −70°C. For reconstitution, 1 mL of 60°C DW was added to the lyophilized cake and vortexed thoroughly.

TPGS/SOL prepared using both methods were centrifuged at 13,000 rpm for 5 min. The supernatant obtained after centrifugation was filtered through a 0.2 μm-pore size filter (Sartorius, Germany). To select a TPGS/SOL capable of encapsulating drugs, mean particle size, polydispersity index (PDI), and zeta potential were measured.

Physicochemical Analysis of Micelles

All size, PDI, and zeta potential measurements were conducted using dynamic light scattering (DLS) (Litesizer 500; Anton Paar, Graz, Austria). For accurate measurement, each sample was diluted 10-fold with DW prior to the analysis.

The determination of encapsulation efficiency (EE, %) for OLA and RAPA was carried out via HPLC and calculated using the following formula:

$$\mathrm{EE}(\%) = \frac{\text{Weight of drug in micelles}}{\text{Weight of feeding drug}} \times 100$$

The results of each analysis were presented as the mean ± standard deviation (SD) based on data obtained from three independent experiments.

To visualize the morphology of OLA/RAPA-TPGS/SOL, transmission electron microscopy (TEM) (JEM-2100, JEOL Ltd., Tokyo, Japan) was employed. Sample preparation for TEM involved depositing a diluted micelle solution onto the center of a copper grid coated with a 200-mesh formvar carbon film. The grid was then air-dried and left to stabilize at 25°C for 2 days. Subsequently, the treated samples were observed using TEM at an acceleration voltage of 200 kV.

In vitro Cytotoxicity Assay

Cytotoxicity assessments were performed using the MTT assay.[65] HeyA8 cells were seeded at a density of 4000 cells/well in 96-well plates and incubated at 37°C in a 5% CO_2 atmosphere for 24 h. Following the incubation period, the cells were exposed to various molar ratios of OLA and RAPA solutions, as well as TPGS/SOL, OLA-TPGS/SOL, RAPA-TPGS/SOL, or OLA/RAPA-TPGS/SOL. A control group, without any drug treatment, was included for comparison. After 48 h incubation, the culture medium was carefully removed. We added 100 μL of MTT solution (concentration of 0.5 mg/mL) to each well, followed by a 4 h incubation. The MTT solution was discarded, and DMSO (100 μL) was added to each well. The plate was then subjected to gentle shaking for 10 min at 200 rpm using an orbital shaker (NB-101S; N-BIOTEK, Bucheon, South Korea), ensuring thorough solubilization of the samples in DMSO. The optical density of the final solution was then quantified at a wavelength of 540 nm, utilizing a microplate reader (Spectra Max ID3; Molecular Devices, San Jose, CA, USA). All data analysis was carried out using GraphPad Prism v 8.4.2 (GraphPad Software, La Jolla, CA, USA).

Drug Interaction Analysis Using Combination Index

The interaction between drugs was assessed using Chou's method, specifically focusing on the combination index (CI).[66] The CI for OLA and RAPA was calculated with the following equation:

$$\text{Combination Index (CI)} = \frac{(D)_1}{(D_x)_1} + \frac{(D)_2}{(D_x)_2}$$

In this equation, $(D_x)_1$ and $(D_x)_2$ represent the inhibitory concentrations of the first and second drug individually, while $(D)_1$ and $(D)_2$ denote the concentrations of each drug when used in combination. A CI value greater than 1 indicates antagonism, less than 1 suggests synergism, and a value equal to 1 implies an additive interaction between the drugs.

Critical Micelle Concentration Determination

TPGS, SOL, and TPGS/SOL loaded with C6 were prepared, and the CMC was assessed using a microplate reader.[67,68] The experiment was performed in triplicate, and fluorescence measurements were conducted with an excitation wavelength of 430 nm and an emission wavelength of 485 nm.

Stability Test

The stability of OLA/RAPA-TPGS/SOL was evaluated in a 4°C refrigerator and 37°C water bath. Samples were collected on days 0, 1, 4, 7, 10, and 14. Each sample, was diluted in a 1:10 ratio with DW for size and PDI determination using DLS instrument, and all experiments were conducted in three replicates.

Stability Assessment of Freeze-Dried Samples for Prolonged Storage

OLA/RAPA-TPGS/SOL, initially prepared using rotary evaporation, underwent a preliminary freezing step in a −70°C deep freezer for 1 h before being subjected to the lyophilization process. All micelle samples intended for long-term storage evaluation were subsequently stored in a −20°C freezer. The samples were rehydrated at specific time points: 0, 1,

7, 14, 30, 60, 100, 120, 150, and 180 days. The measurements conducted at each time point included EE (%), size, PDI, and zeta potential. This experimental procedure was repeated three times.

In vitro Drug Release Assay

The release profiles of OLA/RAPA solutions, and OLA and RAPA from the micelles were determined using the dialysis method.[69] Dialysis membrane bags with a molecular weight cutoff (MWCO) of 20 kD, containing OLA/RAPA solutions, OLA-TPGS/SOL, RAPA-TPGS/SOL or OLA/RAPA-TPGS/SOL, were submerged in 2.0 L of pH 7.4 phosphate-buffered saline (PBS). The OLA/RAPA solution was prepared with 30% Cremophor EL®, 20% EtOH, and 50% DW. The release experiments were conducted with continuous stirring at 200 rpm using a magnetic bar, maintaining a temperature of 37°C. Sample aliquots were collected at designated time points: 0, 2, 4, 6, 8, 24, 48, 72, 168, 240, and 336 h. Each collected sample was diluted 10-fold with acetonitrile and subsequently analyzed using HPLC. To maintain sink conditions, the PBS medium was replenished with fresh medium at 8, 24, 72, 168, and 240 h. These experiments were performed in triplicate. Percentage drug release was determined by curve fitting using the first-order association model with GraphPad Prism v 8.4.2.[70]

In vitro Cellular Uptake of Micelles

For quantitative analysis, HeyA8 cells were seeded in 96-well black plates at a concentration of 2×10^5 cells/well.[71,72] Once the cells reached confluence, they were exposed to 100 μL of C6 solution, C6-loaded SOL, or C6-loaded TPGS/SOL, all at the same concentration. The incubation durations were 1, 2, 4, and 6 h. At the specified time intervals, the culture medium was carefully removed, and the wells were washed thrice with 50 μL of PBS. Following this, each well was treated with 50 μL of a 0.5% Triton X-100 solution in 0.2 N NaOH to induce cell lysis. The fluorescence intensity of each well was measured using a microplate reader, with excitation and emission detection wavelengths at 430 nm and 485 nm, respectively.

Migration Assay

To assess the functional impact of OLA/RAPA-TPGS/SOL treatment on cancer cell migration, we conducted in vitro wound healing assays.[73] HeyA8 cells were seeded in a 24-well plate at a density of 2×10^5 cells/well. When cell confluence reached more than 80%,[74] the unattached cells were gently washed away using DPBS. Subsequently, using a sterile scratcher, a scratch was introduced into the cell monolayer. The cells were then treated with either OLA/RAPA solution or OLA/RAPA-TPGS/SOL, both at the same concentration. At specific time points, images of the scratched area were captured, and the gap width was measured. The initial gap width was considered as 100%.

Preparation of HeyA8 Tumor Spheroids

Regular stem and cancerous tumor cells exhibit notable proliferation and comparable self-renewal patterns.[75–77] Therefore, we prepared HeyA8 tumor spheroids according to our previous studies.[78,79] Briefly, 10 μL of matrigel (Corning, NY, USA) was dispensed into an ultra-low adhesion (ULA) 100 mm dish and 3 μL (1.0×10^4 cells/μL) of cell suspension was added to the matrigel. RPMI 1640 was added to the dish and incubated in a 37°C incubator. The samples were relocated after 24 h to an NB-101SRC orbital shaker (N-BIOTEK, Bucheon, Korea) and incubated for approximately 2 weeks. The morphological characteristics of the tumor spheroids were subsequently observed under a microscope.

In vitro Cytotoxic Effects on HeyA8 Tumor Spheroids

Prior to drug administration, viable cells within the tumor spheroids were measured using an in vivo optical imager (IVIS; VISQUE InVivo Smart-LF, Korea) and quantified using the CleVue™ software (Vieworks, Anyang, Korea) at intervals of 0, 2, 7, 10, and 14 days, specifically targeting live HeyA8 cells and using the Live/Dead Cell Imaging Kit (Thermo Fisher Scientific, Waltham, MA, USA). The cytotoxicity of the formulations against HeyA8 tumor spheroids was performed every other day at the same concentration of OLA-TPGS/SOL, RAPA-TPGS/SOL, or OLA/RAPA-TPGS/SOL. Only the medium was changed on the day of drug administration in the control group.

In vivo Toxicity Test

All animal experiments and protocols have been approved by the Institutional Animal Care and Use Committee (IACUC) of Chungbuk National University (No. CBNUA-2106-23-01; approval date: May 13, 2023) and Samsung Biomedical Research Institute (SBRI), which is an Association for Assessment and Accreditation of Laboratory Animal Care International (AAALAC, protocol No. H-A9-003)-accredited facility, and followed the guidelines of the Laboratory Animal Resource Institute (ILAR).

We employed female ICR mice that were 6 weeks old, obtained from Orientbio Inc. (Sungnam, Korea). The mice were randomly allocated to 11 groups, each consisting of 5 animals. During the experiment, the mice were provided with ample access to both water and food and were subjected to a 1-week acclimatization period. Intravenous administrations were carried out every other day for a duration of 2 weeks. The treatment groups were as follows: control, TPGS/SOL, OLA-TPGS/SOL at doses of 50 mg/kg, 35 mg/kg, and 20 mg/kg, RAPA-TPGS/SOL at doses of 30 mg/kg, 21 mg/kg, and 12 mg/kg, and OLA/RAPA-TPGS/SOL at doses of 50 mg/kg and 30 mg/kg, 35 mg/kg and 21 mg/kg, and 20 mg/kg and 12 mg/kg.

Following the treatment period, the mice were observed for an additional week. Body weights were recorded three times a week at specified intervals. The initial body weight was considered as 100%, and toxicity attributed to the formulation was defined as a loss of more than 20% of body weight, any abnormal behavior, or mortality.[80–82]

In vivo Antitumor Efficacy Evaluation and H&E Staining

To prepare the xenograft model, 6-week-old female BALB/c nude mice (OrientBio, Seongnam, Korea) were purchased and the cells were prepared in two ways.

First, for subcutaneous injection, HeyA8 cells were resuspended in DPBS, and 200 µL (1:1, v/v) of matrigel and cell suspension (2.0×10^6 cells) were injected subcutaneously.[83] For the assessment of antitumor effects, mice were randomly distributed into four groups. Control, OLA-TPGS/SOL, RAPA-TPGS/SOL, and OLA/RAPA-TPGS/SOL, with a dose of 20 mg/kg OLA and 12 mg/kg RAPA. All treatments were injected intravenously via the tail vein every other day, and the control group was not administered. Tumor volume (V) was measured using a caliper and calculated as follows:[84]

$$\text{Tumor Volume (V)} = {}^{1}\!/_{2}\left(Length \times Width^2\right)$$

Mice were sacrificed when tumor volume reached 200 mm^3; mice were monitored every other day, and were sacrificed 3 weeks after cancer cell injection. On the day of sacrifice, the body and tumor weights and, with photographic records of tumors, were documented.

Tumor slides were prepared for H&E staining according to a previously reported methods.[85] The slide images were captured in cross-sectional views at a 20X magnification using the Pannoramic SCANII slide scanner (3DHISTECH, Budapest, Hungary). These images were then processed and analyzed using the CaseViewer 2.7 Software (3DHISTECH).

For the second intraperitoneal injection, HeyA8 cells were injected into the peritoneal cavity of mice at a concentration of 2.5×10^5 cells/0.1 mL HBSS.[86] The experimental groups, drug doses, and methods of administration were all identical to the subcutaneous injection experiments, and the tumor weight and body weight of mice were measured and recorded after sacrifice. Tumors were fixed in formalin and embedded in paraffin or snap frozen in Optimal Cutting Temperature (O.C.T) compound (Sakura Finetek Japan) in liquid nitrogen.

Statistical Analysis

Statistical analysis was performed using an unpaired *t*-test via GraphPad Prism v 8.4.2 software (GraphPad Software, La Jolla, CA, USA). The thresholds for statistical significance were as follows: $*p < 0.05$, $**p < 0.01$, $***p < 0.001$, and $****p < 0.0001$.

Results

Evaluation of Synergistic Effects of OLA and RAPA in HeyA8 Cells

To identify the most effective combination of OLA and RAPA, we determined the 50% inhibition concentration (IC_{50}) values for both drugs in HeyA8 cells and evaluated their CI values.[87] Table 1 and Figure S1 present the IC_{50} values for OLA and RAPA at various molar ratios, illustrating that the efficacy in inhibiting cell growth was influenced by the specific ratio of the combination. As a result of CI analysis, a value of 2.04 was obtained at a molar ratio of 11:1, indicating CI > 1 antagonism. However, for all molar ratios except 11:1 (1:1, 1:2, 1:4, 1:11, 2:1, 2:3, and 4:1), there was synergism with CI < 1 (Figure S2). Therefore, the molar ratio of the drug with the synergistic effect was selected as the optimal ratio and then used to prepare the drug-loaded micelles.

Preparation of TPGS/SOL

TPGS/SOL was prepared using two different methods at different weight ratios (Table 2).

When prepared using a rotary evaporator, the sizes of micelles made with 100 mg and 50 mg of TPGS were 12.7 ± 0.38 nm and 12.9 ± 0.22 nm, respectively, while those of micelles made with 100 mg and 50 mg SOL were 67.4 ± 14.7 nm and 66.1 ± 0.92 nm, respectively.

When the total amount of TPGS/SOL was 100 mg, the size of the micelles with a 4:1 weight ratio was 18.7 ± 0.42 nm, PDI was 0.16 ± 0.02, and zeta potential was −4.33 ± 3.47 mV. When the total amount of TPGS/SOL was 50 mg, the size and PDI were similar, and the zeta potential was 0.00 ± 0.85 mV.

When prepared by freeze-drying, 100 mg and 50 mg TPGS micelles had sizes of 13.2 ± 0.33 nm and 27.1 ± 3.01 nm respectively, and 100 mg and 50 mg SOL micelles had sizes of 68.4 ± 0.71 nm and 66.4 ± 0.13 nm, respectively. At a total amount of 100 mg and a weight ratio of 4:1, the size of the micelles was 18.5 ± 0.16 nm, PDI was 0.17 ± 0.01, and zeta potential was −3.90 ± 1.98 mV. When the total amount of TPGS/SOL was 50 mg, the size and PDI were similar, and the zeta potential was −0.63 ± 0.91 mV.

Therefore, due to the limited solubility of OLA and SOL, a polymer with a lower weight ratio of SOL compared to TPGS was selected for better drug encapsulation.

Preparation of OLA/RAPA-TPGS/SOL

Due to the solubility of OLA in *tert*-butanol,[88] OLA/RAPA-TPGS/SOL were prepared using the thin-film hydration method. EE (%), size, PDI, and zeta potential were evaluated at different total amount of and weight ratios of TPGS and SOL, and at molar ratios of the drugs (Table 3).

Table 1 IC_{50} and CI Values of OLA and RAPA at Various Molar Ratios (n = 3)

Molar Ratio (OLA:RAPA)	IC_{50} (nM)		CI value
	OLA	RAPA	
1:1	147	147	0.03
1:2	323	647	0.17
1:4	62.7	34.6	0.06
1:11	78.1	859	0.20
2:1	403	202	0.08
2:3	110	164	0.04
4:1	282	95.3	0.02
11:1	23,515	2138	2.04

Abbreviations: OLA, olaparib; RAPA, rapamycin; IC_{50}, 50% inhibition concentration; CI, combination index.

Table 2 Physicochemical Properties of TPGS/SOL Prepared from Different Weight Ratios of TPGS and SOL (n = 3, Mean ± SD)

Total amount of TPGS/SOL (mg)	Weight ratio (TPGS:SOL)	Rotary evaporator			Freeze-drying		
		Size (nm)	Polydispersity Index (PDI)	Zeta potential (mV)	Size (nm)	Polydispersity Index (PDI)	Zeta potential (mV)
100	1:0	12.7 ± 0.38	0.07 ± 0.03	−0.10 ± 0.71	13.2 ± 0.33	0.13 ± 0.01	−0.20 ± 2.10
	1:1	69.6 ± 2.08	0.26 ± 0.02	0.87 ± 0.25	91.3 ± 0.94	0.17 ± 0.01	−3.43 ± 1.11
	1:2	78.3 ± 1.80	0.10 ± 0.01	−5.53 ± 3.12	75.9 ± 0.41	0.08 ± 0.01	−2.43 ± 0.70
	1:4	69.0 ± 0.82	0.06 ± 0.03	−2.77 ± 1.33	68.1 ± 0.25	0.18 ± 0.19	−3.77 ± 2.14
	2:1	21.5 ± 3.82	0.23 ± 0.06	−5.53 ± 3.12	21.7 ± 2.72	0.25 ± 0.05	−3.80 ± 2.10
	4:1	18.7 ± 0.42	0.16 ± 0.02	−4.33 ± 3.47	18.5 ± 0.16	0.17 ± 0.01	−3.90 ± 1.98
	0:1	67.4 ± 1.47	0.08 ± 0.03	0.00 ± 1.11	68.4 ± 0.71	0.10 ± 0.02	1.60 ± 0.22
50	1:0	12.9 ± 0.22	0.08 ± 0.03	−0.57 ± 1.31	27.1 ± 3.01	0.30 ± 0.02	−5.20 ± 3.40
	1:1	74.4 ± 11.0	0.22 ± 0.08	−7.00 ± 2.44	84.6 ± 7.44	0.16 ± 0.02	−4.93 ± 2.90
	1:2	79.1 ± 1.94	0.11 ± 0.01	−2.17 ± 0.13	75.7 ± 3.25	0.09 ± 0.02	−3.07 ± 1.93
	1:4	68.3 ± 0.29	0.05 ± 0.12	−1.20 ± 0.83	67.1 ± 1.07	0.05 ± 0.01	−2.60 ± 1.93
	2:1	19.8 ± 1.75	0.18 ± 0.06	2.73 ± 3.37	25.7 ± 5.11	0.29 ± 0.05	−1.20 ± 1.28
	4:1	19.7 ± 0.54	0.17 ± 0.01	0.00 ± 0.85	18.1 ± 1.03	0.11 ± 0.08	−0.63 ± 0.91
	0:1	66.1 ± 0.92	0.06 ± 0.02	0.57 ± 0.05	66.4 ± 0.13	0.06 ± 0.01	0.80 ± 0.29

Abbreviations: TPGS, D-α-tocopheryl polyethylene-glycol (PEG) 1000 succinate; SOL, Soluplus®; PGS/SOL, TPGS/Soluplus micelle.

Table 3 Physicochemical Properties of OLA/RAPA-TPGS/SOL Prepared with Synergistic Drug Ratio (n = 3, Mean ± SD)

Total amount of TPGS/SOL (mg)	Weight ratio (TPGS:SOL)	Molar ratio (OLA:RAPA)	Rotary evaporator				
			Encapsulation Efficiency (EE %)		Size (nm)	PolyDispersity Index (PDI)	Zeta Potential (mV)
			OLA	RAPA			
100	1:1	1:1	44.6 ± 9.13	63.9 ± 6.20	30.1 ± 19.7	0.20 ± 0.06	−2.83 ± 0.29
		1:2	35.3 ± 5.58	64.5 ± 32.2	34.6 ± 7.85	0.16 ± 0.11	−0.17 ± 1.23
		1:4	37.1 ± 1.06	47.1 ± 21.3	18.8 ± 6.17	0.12 ± 0.01	−1.2 ± 1.69
		2:3	37.9 ± 2.67	64.4 ± 2.60	17.5 ± 6.53	0.18 ± 0.01	−0.20 ± 2.10
	2:1	1:1	65.4 ± 12.4	65.9 ± 17.5	58.9 ± 66.6	0.34 ± 0.29	−1.57 ± 1.51
		1:2	44.0 ± 1.65	52.3 ± 1.05	10.6 ± 0.94	0.13 ± 0.03	−4.17 ± 2.52
		1:4	46.9 ± 4.08	39.0 ± 2.45	87.8 ± 103	0.16 ± 0.04	−2.33 ± 1.22
		2:3	44.3 ± 3.58	66.3 ± 3.08	10.4 ± 1.32	0.60 ± 0.37	−2.97 ± 3.13
	4:1	1:1	66.6 ± 0.74	79.3 ± 6.15	16.2± 0.14	0.16 ± 0.01	−0.50 ± 0.43
		1:2	62.6 ± 1.91	73.8 ± 3.52	18.5 ± 8.15	0.12 ± 0.01	−2.27 ± 1.69
		1:4	52.8 ± 1.77	45.7 ± 0.40	23.0 ± 17.0	0.11 ± 0.02	−2.27 ± 1.96
		2:3	66.1 ± 5.95	77.5 ± 5.09	13.4 ± 3.04	0.18 ± 0.06	−5.60 ± 1.02

(*Continued*)

Table 3 (Continued).

Total amount of TPGS/SOL (mg)	Weight ratio (TPGS:SOL)	Molar ratio (OLA:RAPA)	Rotary evaporator				
			Encapsulation Efficiency (EE %)		Size (nm)	PolyDispersity Index (PDI)	Zeta Potential (mV)
			OLA	RAPA			
50	1:1	1:1	41.2 ± 2.62	43.6 ± 2.23	12.1 ± 0.45	0.20 ± 0.01	−8.57 ± 1.75
		1:2	34.3 ± 4.32	26.9 ± 2.49	12.6 ± 0.71	0.17 ± 0.02	−7.90 ± 2.28
		1:4	31.8 ± 1.99	17.5 ± 1.76	15.8 ± 7.45	0.15 ± 0.03	−5.37 ± 3.89
		2:3	32.8 ± 0.65	38.3 ± 1.80	48.5 ± 53.4	0.17 ± 0.02	−6.40 ± 4.56
	2:1	1:1	48.1 ± 1.51	55.2 ± 1.55	119 ± 153	0.46 ± 0.34	−4.83 ± 3.48
		1:2	47.2 ± 0.57	43.5 ± 3.83	14.1 ± 5.04	0.16 ± 0.05	−2.43 ± 1.05
		1:4	41.5 ± 2.45	24.8 ± 0.40	10.3 ± 0.95	0.11 ± 0.02	−1.75 ± 1.25
		2:3	42.4 ± 2.60	59.8 ± 9.52	35.1 ± 30.3	0.21 ± 0.03	−15.7 ± 3.43
	4:1	1:1	48.1 ± 1.51	55.2 ± 1.55	232 ± 191	0.22 ± 0.09	−10.8 ± 7.86
		1:2	52.7 ± 0.17	44.4 ± 0.44	86.2 ± 76.6	0.20 ± 0.01	−20.4 ± 1.15
		1:4	61.3 ± 5.73	76.7 ± 8.12	133 ± 3.11	0.19 ± 0.02	−5.66 ± 1.12
		2:3	54.9 ± 8.87	64.4 ± 6.37	13.0 ± 0.44	0.18 ± 0.01	−11.6 ± 0.63

Abbreviations: TPGS, D-α-tocopheryl polyethylene-glycol (PEG) 1000 succinate; SOL, Soluplus®; OLA, olaparib; RAPA, rapamycin.

The EE (%) of OLA was higher when the amount of polymer was 100 mg than 50 mg. The EE (%) of OLA at a polymer weight ratio of 1:1 was <55%. The size measured at the polymer weight ratio of 4:1 was <30 nm, and the PDI was ≤0.2. In this weight ratio, the EE (%) of OLA and RAPA at a drug molar ratio of 2:3 were 66.1 ± 5.95% and 77.5 ± 5.09%, respectively, and the zeta potential was −5.60 ± 1.02 mV. Considering all the conditions evaluated, a TPGS/SOL with a total amount of 100 mg and a weight ratio of 4:1 was selected, and a drug encapsulated at a molar ratio of 2:3 was finally selected.

Figure 2A and B show the size distribution of OLA/RAPA-TPGS, OLA/RAPA-SOL, and OLA/RAPA-TPGS/SOL. The size of OLA/RAPA-SOL was >20000 nm, whereas the size of OLA/RAPA-TPGS/SOL was <20 nm. The PDI of OLA/RAPA-TPGS and OLA/RAPA-SOL was >0.2, whereas the PDI of OLA/RAPA-TPGS/SOL was <0.2. Furthermore, TEM images revealed that the micelles possessed a consistent spherical shape.

Critical Micelle Concentration (CMC) Determination

To evaluate the self-aggregation capacity of TPGS, SOL, and TPGS/SOL, the CMC was measured[89] and is presented in Figure 2C–E. TPGS exhibited the highest CMC value of 0.033 mg/mL, while SOL exhibited the lowest value of 0.016 mg/mL. The mixed micelles of TPGS/SOL exhibited a value of 0.021 mg/mL.

Stability Test

The size and PDI of OLA/RAPA-TPGS/SOL were monitored at both 4°C and 37°C for 2 weeks period (Figure 3A and B). At 4°C, the size remained consistently below 30 nm by day 10, and the PDI was <0.2 by day 7. When stored at 37°C, the size was maintained below 200 nm by day 10, and the PDI was remained below 0.2 by day 7.

Stability Assessment of Freeze-Dried Samples for Prolonged Storage

Physicochemical characteristics of OLA and RAPA encapsulated in TPGS/SOL evaluated after 180 days of storage (Figure 3C–G) (Table S1). The EE (%) of day 0 OLA and RAPA were 75.1 ± 3.53% and 86.4 ± 9.43%, respectively.

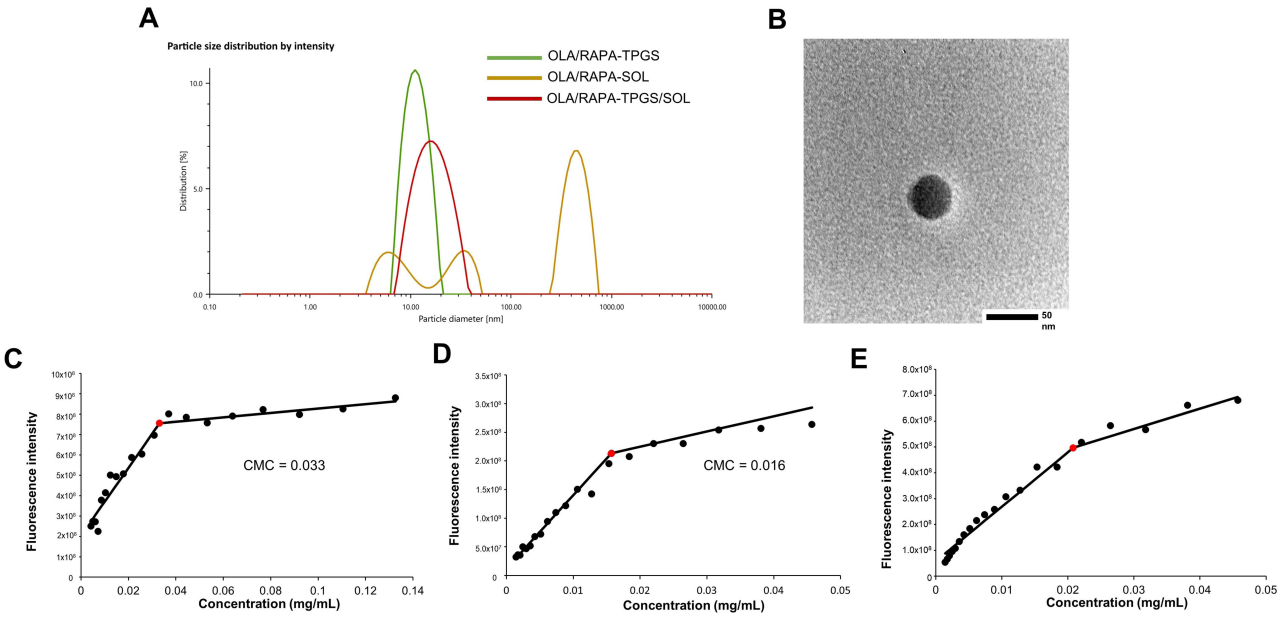

Figure 2 (**A**) Representative size distribution of TPGS/SOL, OLA/RAPA-TPGS micelle, OLA/RAPA-SOL, and OLA/RAPA-TPGS/SOL. (**B**) Transmission electron microscopy (TEM) images of OLA/RAPA-TPGS/SOL. CMC graphs of (**C**) TPGS, (**D**) SOL, and (**E**) TPGS/SOL.
Abbreviations: TPGS, D-α-tocopheryl polyethylene-glycol (PEG) 1000 succinate; SOL, Soluplus®; OLA, olaparib; RAPA, rapamycin; CMC, critical micelle concentration.

On day 180, the EE (%) of OLA and RAPA were 54.9 ± 12.2% and 63.6 ± 13.8%, respectively. The size was evaluated as 13.1 ± 3.91 at day 0 and 14.6 ± 0.43 at day 180, and the PDI was 0.14 ± 0.03 and 0.12 ± 0.01, respectively. In addition, the zeta potential was measured as −5.37 ± 0.33 mV and 0.33 ± 1.04 mV on the first and last day of evaluation, respectively. No significant differences were observed in the EE (%), size, PDI, and zeta potential values of the formulations on day 0 and day 180.

In vitro Drug Release Assay

The release profiles of OLA/RAPA solution, OLA-TPGS/SOL, RAPA-TPGS/SOL and OLA/RAPA-TPGS/SOL were analyzed (Figure 4), and their first order rate constants (k, h^{-1}) were calculated. The calculated k values for OLA release were 0.14, 0.02, and 0.03 for OLA/RAPA solution, OLA-TPGS/SOL, and OLA/RAPA-TPGS/SOL, respectively. The corresponding k values for RAPA release were 0.15, 0.03, and 0.02 for OLA/RAPA solution, RAPA-TPGS/SOL, and OLA/RAPA-TPGS/SOL.

At 6 h, the percentage of OLA released were 71.4 ± 5.06%, 28.5 ± 14.0%, and 25.8 ± 12.6% for OLA/RAPA solution, OLA-TPGS/SOL, and OLA/RAPA-TPGS/SOL, respectively. At 72 h, these percentages increased to 92.7 ± 0.56%, 83.2 ± 4.46%, and 56.5 ± 8.70%, respectively. By 336 h, 96.9 ± 4.24%, 96.8 ± 3.29%, and 69.9 ± 4.00% OLA had been released, respectively.

Comparing the release rates of OLA from OLA/RAPA solution and OLA/RAPA-TPGS/SOL, a significantly slower release was observed at 6, 8, 24, 48, and 240 h in the latter (*$p < 0.05$, *$p < 0.05$, **$p < 0.01$, ***$p < 0.001$, and *$p < 0.05$). Similarly, comparing OLA release rates from OLA-TPGS/SOL and OLA/RAPA-TPGS/SOL significant differences were observed at 48, 72, 168, 240, and 336 h (*$p < 0.05$, *$p < 0.05$, *$p < 0.05$, **$p < 0.01$, and **$p < 0.01$).

For RAPA, at 24 h, 81.1 ± 3.59%, 55.2 ± 1.23%, and 30.3 ± 13.0% of the drug was released from OLA/RAPA solution, RAPA-TPGS/SOL, and OLA/RAPA-TPGS/SOL, respectively. At 336 h, 98.8 ± 1.67%, 99.9 ± 0.01%, and 80.8 ± 13.9% of RAPA had been released, respectively.

Comparing the release rates of RAPA from OLA/RAPA solution and OLA/RAPA-TPGS/SOL, a significantly slower release was observed at 6, 8, 24, 48, and 72 h in the latter (**$p < 0.01$, **$p < 0.01$, **$p < 0.01$, *$p < 0.05$, and *$p < 0.05$). Additionally, there was a significantly slower release from OLA/RAPA-TPGS/SOL at 72 and 168 h compared than that from RAPA-TPGS/SOL (*$p < 0.05$ and *$p < 0.05$).

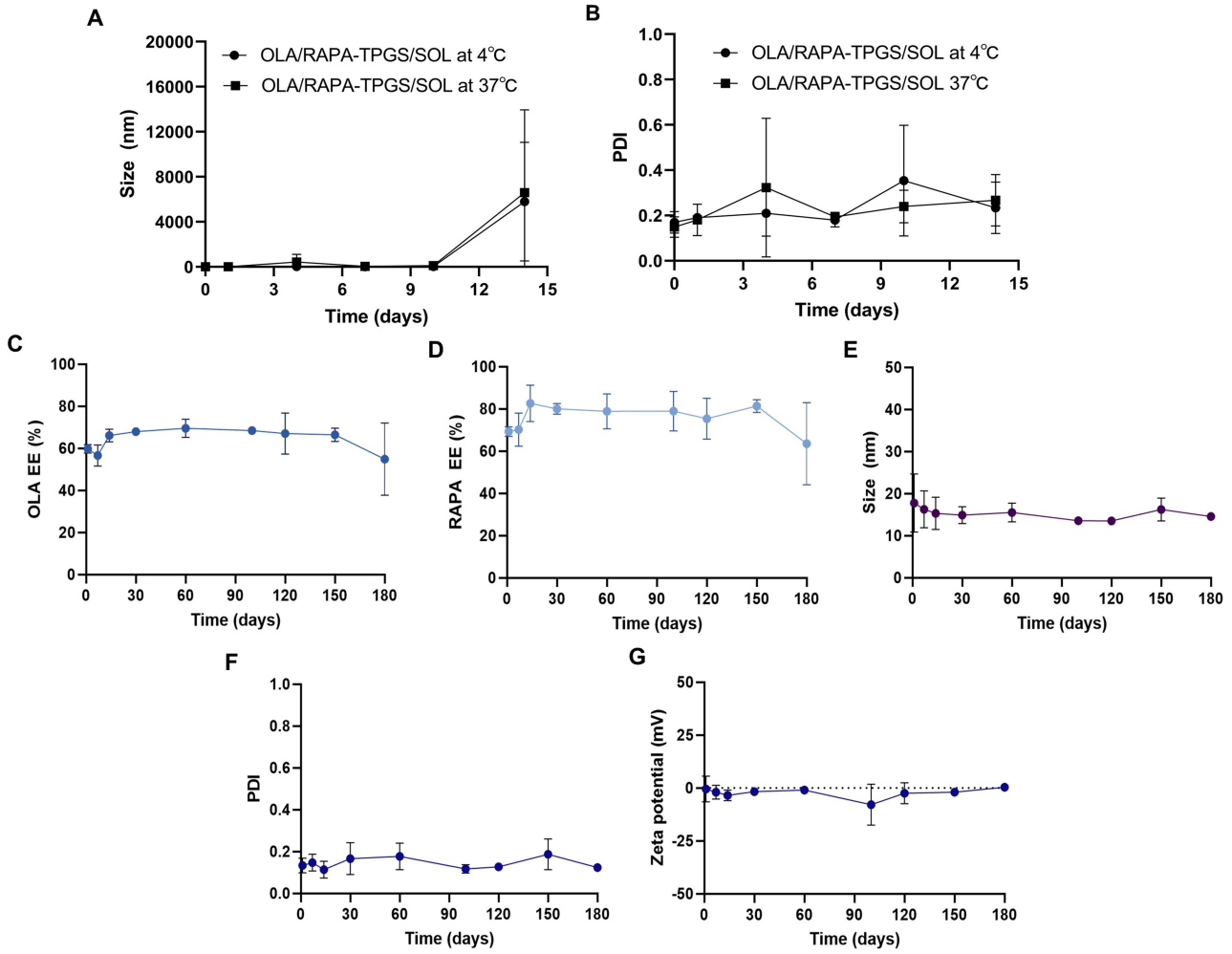

Figure 3 Changes in (**A**) mean particle size and (**B**) PDI of OLA/RAPA-TPGS/SOL during short-term stability evaluation at 4°C and 37°C, and (**C**) OLA EE (%), (**D**) RAPA EE (%), (**E**) size, (**F**) PDI, and (**G**) zeta potential of OLA/RAPA-TPGS/SOL during long-term stability evaluation.
Abbreviations: OLA, olaparib; RAPA, rapamycin; TPGS, D-α-tocopheryl polyethylene glycol 1000 succinate; SOL, Soluplus®.

In vitro Cytotoxicity Assay

Figure 5A–F shows the cytotoxicity of free OLA, free RAPA, TPGS/SOL, OLA-TPGS/SOL, RAPA-TPGS/SOL and OLA/RAPA-TPGS/SOL. The IC_{50} values of free OLA and free RAPA were 15355 nM and 3881 nM, respectively. The IC_{50} values of TPGS/SOL, OLA-TPGS/SOL, RAPA-TPGS/SOL, and OLA/RAPA-TPGS/SOL were 1435 nM, 308 nM, 77.8 nM, and 148 nM, respectively.

In vitro Cellular Uptake of the Micelles

The quantitative cellular uptake of HeyA8 cells after incubation with the C6 solution, C6-SOL and C6-TPGS/SOL are shown in Figure 5G. At 2 h, the fluorescence intensities were 10358566 ± 157,272, 22,583,551 ± 994029, and 31021971 ± 2964196, respectively. C6-TPGS/SOL showed higher fluorescence intensity compared to C6 solution and C6-SOL, which was statistically significant (***$p < 0.001$ and *$p < 0.05$). Furthermore, the fluorescence intensities at 6 h were 22568195 ± 317,796, 45,433,855 ± 8371219, and 74868389 ± 3391258 for C6, C6-SOL, and C6-TPGS/SOL, respectively. At 6 h, C6-TPGS/SOL showed higher fluorescence intensity than that of C6 solution and C6-SOL, which was statistically significant (**$p < 0.01$ and ****$p < 0.0001$).

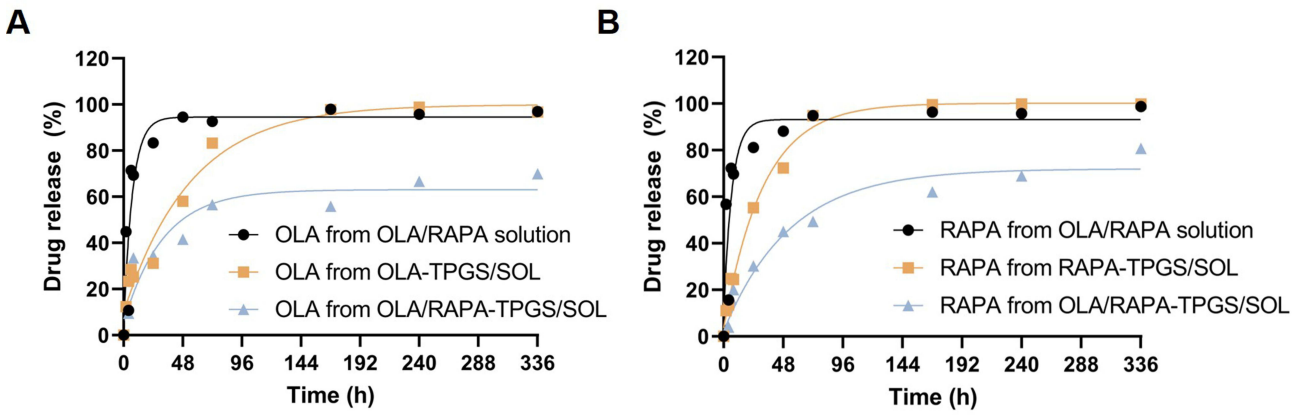

Figure 4 OLA/RAPA solution, single and combined drug release profiles of OLA and RAPA in micelles. (**A**) OLA release in OLA/RAPA solution, OLA-TPGS/SOL and OLA/RAPA-TPGS/SOL, and (**B**) RAPA release in OLA/RAPA solution, RAPA-TPGS/SOL and OLA/RAPA-TPGS/SOL (n = 3).
Abbreviations: TPGS, D-α-tocopheryl polyethylene-glycol (PEG) 1000 succinate; SOL, Soluplus®; OLA, olaparib; RAPA, rapamycin.

Migration Assay

To observe cell migration, the scraped cells were incubated with cell medium, free OLA/RAPA or OLA/RAPA-TPGS/SOL (Figure 5H and I). The gap width of the control was 62.4 ± 5.06% and 5.76 ± 8.13% at 8 and 24 h, respectively, while the gap width of free OLA/RAPA was 69.9 ± 1.84% and 5.35 ± 6.18%, respectively. The 2, 8, and 24 h gap widths of OLA/RAPA-TPGS/SOL were measured to be 93.4 ± 4.07%, 84.3 ± 7.65% and 65.2 ± 20.9%, respectively. The OLA/RAPA-TPGS/SOL after 8 h showed wider intercellular spacing compared to the control and free OLA/RAPA groups, which was statistically significant (*$p < 0.05$ and **$p < 0.01$). In addition, the OLA/RAPA-TPGS/SOL after 24 h showed significantly wider intercellular spacing compared to the control and free OLA/RAPA groups (**$p < 0.01$ and **$p < 0.01$).

In vitro Cytotoxic Effects on HeyA8 Tumor Spheroids

The HeyA8 tumor spheroids were observed at various time (days 0, 2, 7, 10, and 14) under a microscope (Figure S4). These HeyA8 tumor spheroids were then subjected to treatments with OLA-TPGS/SOL, RAPA-TPGS/SOL, or OLA/RAPA-TPGS/SOL (Figure 6A). The degree of spheroids growth suppression was quantified using the IVIS system (Figure 6B).

On day 2, the total flux of tumor spheroids treated with OLA-TPGS/SOL, RAPA-TPGS/SOL, and OLA/RAPA-TPGS/SOL had decreased by 7.07%, 17.3% and 47.5%, respectively, in comparison to day 0. Subsequently, this reduction became more pronounced, reaching 80.3%, 81.2%, and 91.8%, respectively, on day 14. In contrast, the total flux of tumor spheroids in the control group increased by 127% over the same period. On the last day of the evaluation, the OLA/RAPA-TPGS/SOL group had reduced the total flux of tumor spheroids by 15.6-fold compared to the by the control group (***$p < 0.001$) (Figure 6C).

In vivo Toxicity Test

Figure 7 shows weight change and survival after administration of single and combination micelles of OLA and RAPA at various doses. The two groups that were administered 50 mg/kg OLA (OLA-TPGS/SOL and OLA/RAPA-TPGS/SOL) showed a survival rate of 60%.

No weight loss of more than 20% from initial body weight and no deaths were observed in any of the other groups.

In vivo Antitumor Efficacy and H&E Staining

The antitumor efficacy of OLA/RAPA-TPGS/SOL was evaluated by subcutaneous and intraperitoneal administration to HeyA8 cell xenograft model mice.[83,86] When assessed by subcutaneous cell injection, tumors in the OLA/RAPA-TPGS/SOL group were inhibited by 36.6% on day 14 compared with that day 0, which is 21.6-, 2.57-, and 1.76-times more than

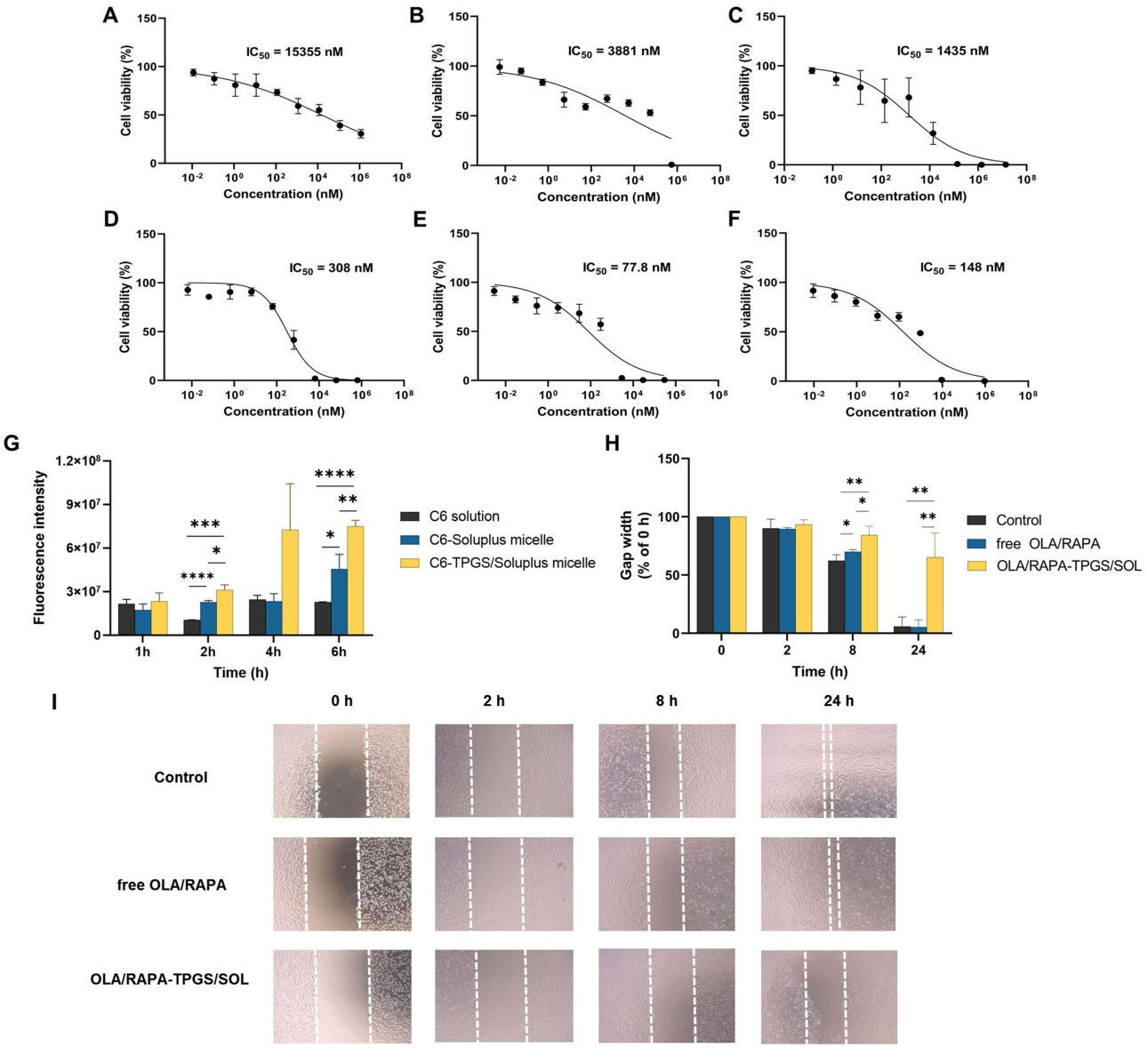

Figure 5 In vitro cytotoxicity assay of HeyA8 cells treated with (**A**) free OLA, (**B**) free RAPA, (**C**) TPGS/SOL, (**D**) OLA-TPGS/SOL, (**E**) RAPA-TPGS/SOL, and (**F**) OLA/RAPA-TPGS/SOL. (**G**) Cellular uptake efficiency in HeyA8 ovarian cancer cells incubated with equivalent C6 concentrations of C6 solution, C6-SOL, and C6-TPGS/SOL (n = 3). (**H**) Graph and (**I**) microscopic images of wound healing assays using control, free OLA/RAPA, and OLA/RAPA-TPGS/SOL. (*$p < 0.05$, **$p < 0.01$, ***$p < 0.001$, and ****$p < 0.0001$).

Abbreviations: TPGS, D-α-tocopheryl polyethylene-glycol (PEG) 1000 succinate; SOL, Soluplus®; OLA, olaparib; RAPA, rapamycin.

that of the control, OLA-TPGS/SOL, and RAPA-TPGS/SOL groups, respectively (****$p < 0.0001$, ***$p < 0.001$, and *$p < 0.05$) (Figure 8A). Moreover, tumor weight was the lowest in OLA/RAPA-TPGS/SOL at, 0.38 ± 0.18 g (Figure 8B and C). Figure 8D and E show no reduction in body weight and survival rate. Tumor H&E staining showed that the density of cells in the control group remained uniform, and no necrotic areas or abnormal tissue deformation were observed (Figure 9). Conversely, in the OLA/RAPA-TPGS/SOL group, area of apoptosis and necrosis were identified, accompanied by decreased cell density. When evaluated by cell injection into the abdominal cavity, the tumor weight of the OLA/RAPA-TPGS/SOL group was 0.61 ± 0.41 g, which is significantly lower than that of the control group, which was 1.64 ± 0.86 g (**$p < 0.01$) (Figure S6A). In addition, there was no significant difference in body weight compared with the control in any group (Figure S6B).

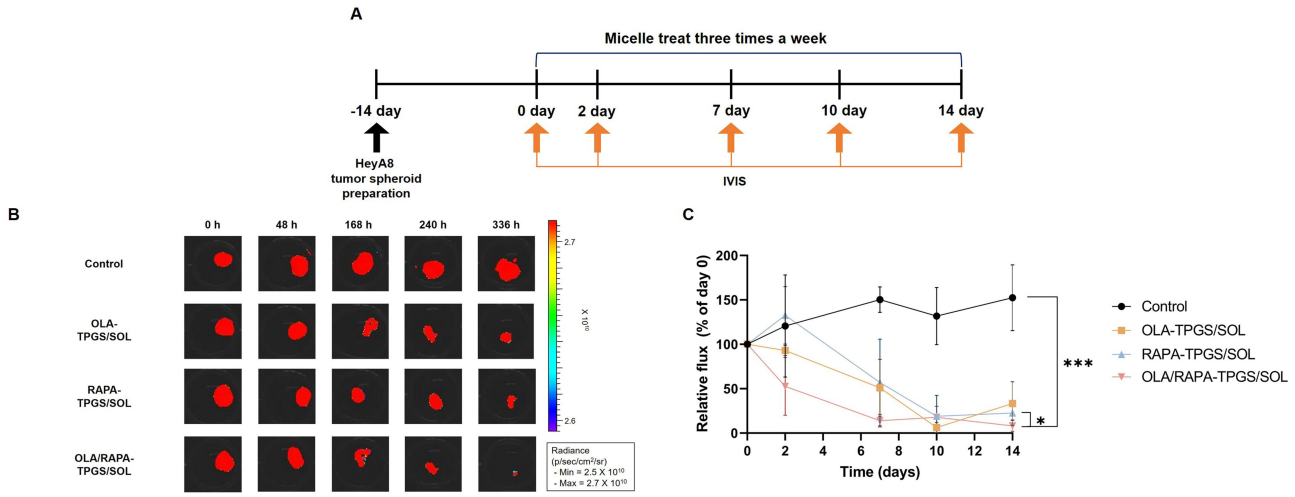

Figure 6 (**A**) Time schedule of cytotoxicity assay using HeyA8 tumor spheroids, (**B**) representative IVIS images of tumor spheroids treated with micelles, and (**C**) total flux values (p/sec) compared to day 0. (*$p < 0.05$ and ***$p < 0.001$).

Abbreviations: TPGS/SOL, TPGS/Soluplus micelle; TPGS, D-α-tocopheryl polyethylene-glycol (PEG) 1000 succinate; SOL, Soluplus®; OLA, olaparib; RAPA, rapamycin.

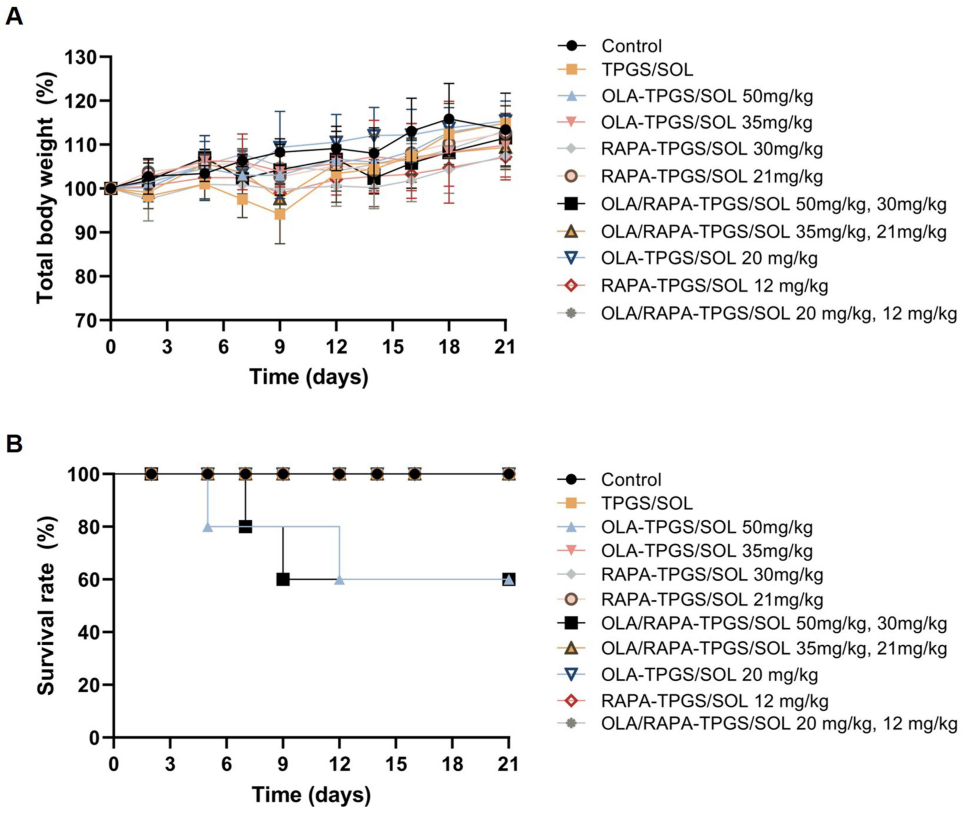

Figure 7 Graphs of (**A**) relative body weight changes and (**B**) survival rates for the toxicity test using control, TPGS/SOL, and single and co-loaded micelles with different doses of OLA and RAPA.

Abbreviations: OLA, olaparib; RAPA, rapamycin; TPGS, D-α-tocopheryl polyethylene-glycol (PEG) 1000 succinate; SOL, Soluplus®.

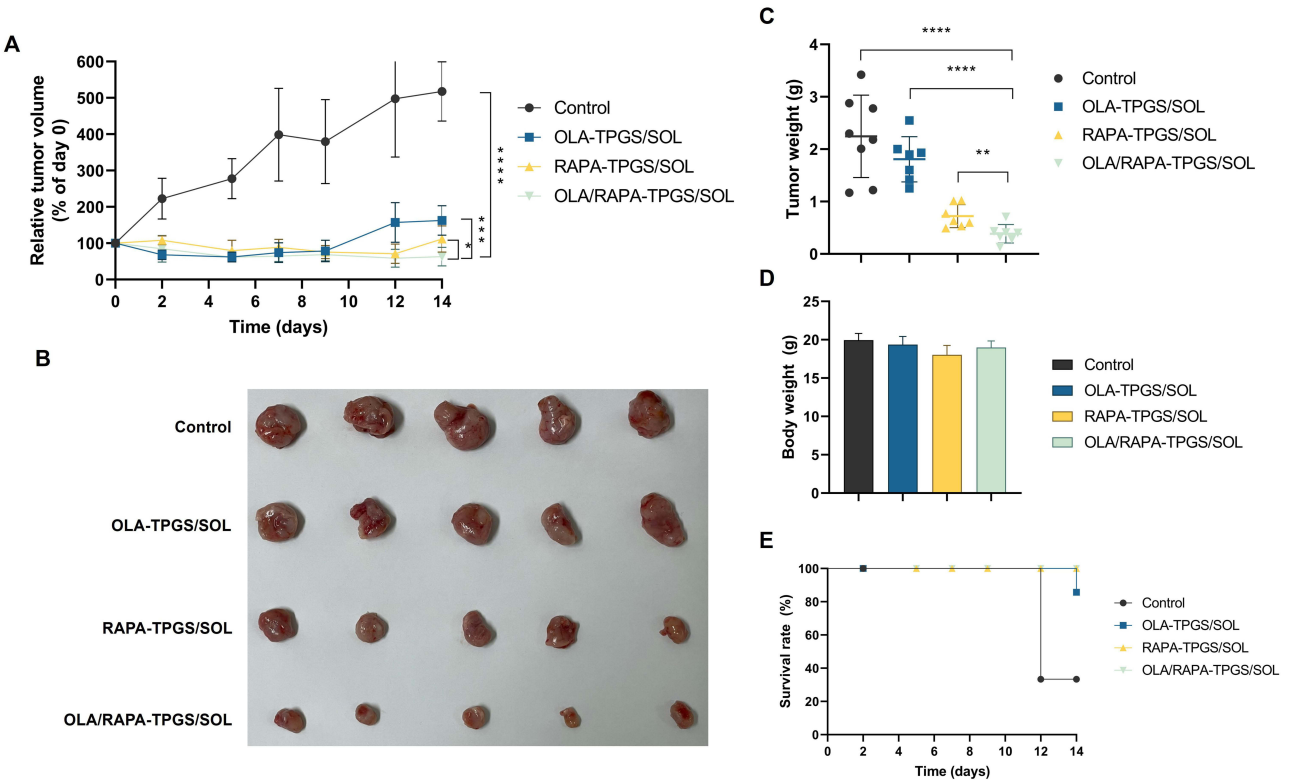

Figure 8 Anticancer efficacy in a HeyA8 cell subcutaneous xenograft model based on (**A**) tumor volume (**B**) tumor image, (**C**) tumor weight, (**D**) body weight, and (**E**) survival rate. (*p < 0.05, **p < 0.01, ***p < 0.001, and ****p < 0.0001).
Abbreviations: OLA, olaparib; RAPA, rapamycin; TPGS, D-α-tocopheryl polyethylene-glycol (PEG) 1000 succinate; SOL, Soluplus®.

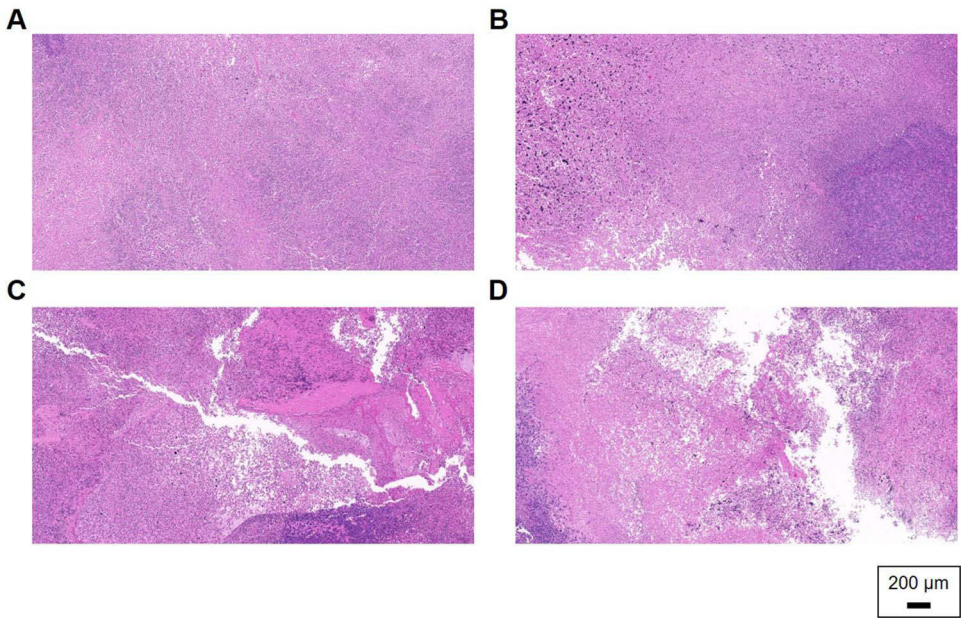

Figure 9 Representative images of H&E staining for (**A**) control, (**B**) OLA-TPGS/SOL, (**C**) RAPA-TPGS/SOL, and (**D**) OLA/RAPA-TPGS/SOL.
Abbreviations: OLA, olaparib; RAPA, rapamycin; TPGS, D-α-tocopheryl polyethylene-glycol (PEG) 1000 succinate; SOL, Soluplus®.

Discussion

PARP enzymes play crucial roles in cellular processes, including DNA repair, replication and apoptosis. In contrast, the mTOR pathway affects many cellular activities, including the regulation of cell growth, proliferation, and angiogenesis.[90,91] Therefore, we hypothesized that combination treatment with OLA, a PARP inhibitor, and RAPA, an mTOR inhibitor, would be effective against ovarian cancer. However, OLA and RAPA exhibit limited bioavailability due to their poor water solubility.[21,30,92] To enhance their solubility and bioavailability, we prepared polymeric micelles, particularly mixed micelles, which offer the advantages of improved micelle stability and EE (%).[54,93,94] In addition, as reported in a previous paper, mixed micelles prevent rapid drug release by modulating the CMC.[54]

Although various molar ratios of OLA and RAPA showed synergistic effects, 1:1, 1:2, 1:4 and 2:3 molar ratios were selected for incorporation into the micelles due to the solubility of OLA. At TPGS and SOL weight ratios of 1:1 and 2:1, the EE (%) of most of OLA was significantly lower at <50%, so a 4:1 weight ratio of TPGS and SOL was selected for the micelles. The micelles, formulated with an OLA/RAPA molar ratio of 2:3 and a TPGS/SOL weight ratio of 4:1, exhibited particle sizes under 20 nm and a zeta potential of −5.60 ± 1.02 mV. These properties are anticipated to facilitate enhanced tumor accumulation compared to normal tissues, owing to the EPR effect, while also demonstrating a reduced rate of macrophage uptake[95,96] In addition, the particle size of OLA/RAPA-TPGS/SOL was maintained at <200 nm until 10 days when evaluated in the liquid state for 14 days, and no significant difference in physicochemical properties from day 0 was observed until 180 days when stored in the solid state for a long time. Therefore, freeze-drying the formulation prepared by rotary evaporator and long-term storage at −20°C is recommended.[97]

The results of the MTT assay showed that the IC_{50} value of TPGS/SOL was lower than that of free OLA and RAPA.[98] This may be because TPGS induces apoptosis and inhibits cell proliferation;[99–101] however, it has been reported that it is not toxic in normal cells.[102,103] The IC_{50} value of RAPA-TPGS/SOL was lower than that of OLA/RAPA-TPGS/SOL, indicating that the cytotoxicity effect of the formulations may be due to the faster release of the drug from RAPA-TPGS/SOL, with RAPA release after 48 h (drug treatment time in the MTT assay) of 72.4 ± 7.69% and 45.0 ± 19.8%, respectively. Furthermore, OLA-TPGS/SOL showed lower IC_{50} values than free OLA (**$p < 0.01$), RAPA- TPGS/SOL showed lower IC_{50} values than free RAPA (**$p < 0.01$), and OLA/RAPA-TPGS/SOL showed higher cytotoxicity than free OLA/RAPA (**$p < 0.01$). In the cell migration assay, the final formulation showed the most inhibited cell migration capacity compared to the control and free OLA/RAPA, which is consistent with the cytotoxicity test results. Therefore, OLA/RAPA-TPGS/SOL can block apoptosis and tumor cell motility.[74] The P-gp inhibition ability of TPGS has been reported in several papers. Accordingly, as a result of C6-SOL and C6-TPGS/SOL in culture with HeyA8 cells, significance was shown at 2 and 6 h (*$p < 0.05$ and **$p < 0.01$), and the intracellular level of mixed micelles containing TPGS increased rapidly. Therefore, TPGS can enhance the intracellular levels of the enclosed drug, increasing drug accumulation inside tumor cells.[104,105] In addition, since non-multidrug-resistant cancer cells do not have the same level of drug efflux mechanisms as MDR cancer cells, they can allow the drug to accumulate inside the cells more effectively, thereby improving the therapeutic efficacy of the drug.[106,107] The particle size of OLA/RAPA-TPGS and OLA/RAPA-TPGS/SOL was measured to be <50 nm, while the particle size of OLA/RAPA-SOL was >20000 nm. Several studies have reported that the optimal size of nanoparticles to achieve the highest cellular uptake is <50 nm,[108] suggesting that TPGS/SOL is likely to contribute to increased intracellular levels.

The release rates of OLA were compared in OLA/RAPA solution, OLA-TPGS/SOL, and OLA/RAPA-TPGS/SOL, and the release rates of RAPA were compared in OLA/RAPA solution, RAPA-TPGS/SOL, and OLA/RAPA-TPGS/SOL. OLA was >95% released from OLA/RAPA solution and OLA-TPGS/SOL at 240 h, however, <70% released from OLA/RAPA-TPGS/SOL, indicating a significant difference (*$p < 0.05$ and **$p < 0.01$). RAPA was >90% released from OLA/RAPA solution and RAPA-TPGS/SOL at 72 h, however, <70% released from OLA/RAPA-TPGS/SOL, showing a significant difference (*$p < 0.05$ and *$p < 0.05$). Comparing the release of OLA/RAPA solution and OLA/RAPA-TPGS/SOL, significant differences were found at several time points, suggesting that the drug is trapped in the micelles, limiting the rapid release of the drug.[109,110] Micelles carriers loaded with hydrophobic drugs have been shown to increase the solubility of the drug and allow for a slower release of the drug.[111] Furthermore, the analysis of release patterns between combined and individual micelles revealed significant disparities at certain points, hinting at the likelihood of

hydrophobic drug interactions within the core of the micelles.[112] In addition, the lack of initial explosive release from OLA/RAPA-TPGS/SOL indicates that in vivo toxicity can be prevented.[113,114] Finally, CMC measurements showed that the TPGS and SOL mixed micelles had comparatively lower CMC values than that of the TPGS, suggesting that the mixing of the polymers may make the micelles more stable in the blood[115–117] In addition, it suggests that they dissociate relatively slowly in the blood, which is consistent with the results of in vitro release tests showing that OLA/RAPA-TPGS/SOL release OLA and RAPA slower than OLA/RAPA-TPGS (Figure S3).[102,103]

The in vivo toxicity evaluation showed no reduction in body weight and survival with TPGS/SOL administration, suggesting that TPGS/SOL are nontoxic. Several studies have reported that TPGS and SOL are not toxic.[118,119] OLA-TPGS/SOL (50 mg/kg) and OLA/RAPA-TPGS/SOL (50 mg/kg, 30 mg/kg) showed a 60% survival rate, but RAPA-TPGS/SOL (30 mg/kg) showed no change in body weight and no decrease in survival. This suggests toxicity at 50 mg/kg OLA. Weight change and decreased survival were not seen in any of the groups except for the higher dose of OLA, indicating no toxicity.[120]

To evaluate cytotoxicity in 3D structures, formulations were evaluated using tumor spheroids. After 2 weeks, OLA/RAPA-TPGS/SOL significantly inhibited more cells compared to RAPA-TPGS/SOL group ($*p < 0.05$). Contrary to the results of the MTT assay, which showed that the IC_{50} of RAPA-TPGS/SOL was lower than that of the final formulations, the final formulation inhibited tumors to the greatest extent in tumor spheroids. This is likely due to the difference between 2D and 3D models. 3D models of cells have been reported to have the same cell density as natural tissues and show a similar drug response to solid tumor.[121] In addition, in an in vivo anti-cancer efficacy evaluation conducted during the same period, OLA/RAPA-TPGS/SOL showed the greatest tumor inhibition compared to all other groups (Figure S5 and Figure S6). The tumor weight in the OLA/RAPA-TPGS/SOL group was significantly lower than in the control, OLA-TPGS/SOL, and RAPA-TPGS/SOL groups ($****p < 0.0001$, $****p < 0.0001$, and $**p < 0.01$) with no decrease in survival rate. These results suggest that, first, the two drugs were delivered simultaneously to the tumor in the designed proportions, possibly resulting in synergistic effect of the drugs.[122,123] Second, TPGS may have enhanced the cellular uptake of the drugs, increasing their cytotoxicity against cancer cells.[124,125] Finally, the lack of decreased survival rate in mice suggests that mixed micelle, OLA, and RAPA did not exhibit toxicity.[126,127] H&E analysis confirmed the uniform cell density in the control group, whereas cell death was observed in the periphery in the drug-treated group. In particular, significant tissue structure changes were observed in the OLA/RAPA-TPGS/SOL-treated tumor tissue compared to the control group. Moreover, areas of apoptosis and necrosis were identified, indicating a decrease in cell density. This suggest that OLA/RAPA-TPGS/SOL exerts an anticancer effect in ovarian cancer and that the combined treatment of OLA and RAPA has a synergistic effect against tumor cells.[128,129]

Conclusions

This study encapsulated OLA and RAPA in micelles to address the issue of low solubility. This approach not only improved the solubility of both drugs but also enhanced intracellular drug delivery efficiency through TPGS, resulting in an efficient formulation. Typically, dissolving poorly soluble drugs requires toxic solubilizing agents, which raises concerns about side effects. However, the use of micelles effectively mitigated this issue. Additionally, the OLA/RAPA-TPGS/SOL micelles demonstrated high stability and exhibited significant anticancer efficacy with low toxicity in both in vitro and in vivo experiments. These findings underscore the novelty and potential of our formulation.

Abbreviations

PARP, poly(ADP-ribose) polymerase; Olaparib, OLA; HR, homologous recombination; mTOR, mammalian target of rapamycin; PEG, D-α-tocopheryl polyethylene-glycol; TPGS, D-α-tocopheryl polyethylene-glycol 1000 succinate; TOS, α-tocopheryl succinate; P-gp, P-glycoprotein; MDR, multiple drug resistance; SOL, soluplus®; CMC, critical micelle concentration; EPR, enhanced permeability and retention; 3D, three-dimensional; 2D, two-dimensional; C6, coumarin 6; MTT, thiazolyl blue tetrazolium bromide; NaOH, sodium hydroxide solution; DMSO, dimethyl sulfoxide; EtOH, ethanol; DW, distilled water; HPLC, high-performance liquid chromatography; FBS, fetal bovine serum; RPMI 1640, Roswell Park Memorial Institute 1640; DPBS, Dulbecco's phosphate buffered saline; PDI, polydispersity index; TPGS/SOL, only TPGS and SOL without drug loading; OLA/RAPA-TPGS/SOL, TPGS/SOL micelles loaded with OLA and

RAPA; DLS, dynamic light scattering; EE (%), encapsulation efficiency; TEM, transmission electron microscopy; CI, combination index; PBS, phosphate-buffered saline; ULA, ultra-low adhesion; IACUC, institutional animal care and use committee; V, tumor volume; IC_{50}, 50% inhibition concentration.

Data Sharing Statement

All the data contained in the article is available.

Ethics Approval

This experimental protocols and animal experiments were performed with the approval of the Institutional Animal Care and Use Committee (IACUC) of Chungbuk National University (No. CBNUA-2106-23-01; approval date: May 13, 2023). Also, this experiment was reviewed and approved by the IACUC of Samsung Biomedical Research Institute (protocol No. H-A9-003), which is an accredited facility by the Association for Assessment and Accreditation of Laboratory Animal Care International (AAALAC) and abides by the Institute of Laboratory Animal Resources (ILAR) guideline. Treatment and welfare of laboratory animals were in accordance with the guidelines of the Ministry of Food and Drug Safety (MFDS) in the Republic of Korea.

Author Contributions

Conceptualization, Y.B.S. and D.H.S.; methodology, Y.B.S. and M.S.Y.; software, Y.B.S.; validation, Y.B.S. and D.H.S; formal analysis, Y.B.S.; investigation, Y.B.S.; resources, D.H.S.; data curation, Y.B.S., M.S.Y., M.K.Y., J.Y.C., J.W.L., and D.H.S.; interpretation, Y.B.S., M.S.Y., M.K.Y., J.Y.C., J.W.L., and D.H.S.; writing-original draft preparation, Y.B.S.; writing-review and editing, Y.B.S., M.S.Y., M.K.Y., J.Y.C., J.W.L., and D.H.S.; visualization, Y.B.S.; super-vision, J.W.L. and D.H.S.; project administration, Y.B.S., M.S.Y., M.K.Y., J.Y.C., J.W.L., and D.H.S. All authors made substantial contributions to conception and design, acquisition of data, or analysis and interpretation of data; took part in drafting the article or revising it critically for important intellectual content; agreed to submit to the current journal; gave final approval of the version to be published and agree to be accountable for all aspects of the work.

Funding

This research was supported by "Regional Innovation Strategy (RIS)" through the National Research Foundation of Korea (NRF) funded by the Ministry of Education (MOE) (2021RIS-001). This research was funded by the Basic Science Research Program through the National Research Foundation of Korea (NRF), funded by the Ministry of Education, grant number NRF-2022R1C1C1007107. This work was supported by the the Ministry of Science and ICT, (2024-22030007-30) and Commercialization Promotion Agency for R&D Outcomes(COMPA); and under the framework of international cooperation program managed by the National Research Foundation of Korea (2022K2A9A2A0800016412). This study was supported by SMC-SKKU Future Convergence Research Program Grant (SMO1231041).

Disclosure

Professor Dae Hwan Shin reports a pending patent "TPGS/Soluplus Micelles containing olaparib and rapamycin, and uses thereof". The authors report no other conflicts of interest in this work.

References

1. Siegel RL, Miller KD, Fuchs HE, Jemal A. Cancer statistics, 2021. *Ca Cancer J Clin*. 2021;71(1):7–33.
2. Li -S-S, Ip CK, Tang MY, et al. Sialyl Lewisx-P-selectin cascade mediates tumor–mesothelial adhesion in ascitic fluid shear flow. *Nat Commun*. 2019;10(1):2406.
3. Lheureux S, Gourley C, Vergote I, Oza AM. Epithelial ovarian cancer. *Lancet*. 2019;393(10177):1240–1253.
4. Piver MS. Treatment of ovarian cancer at the Crossroads:--50 years after single-agent melphalan chemotherapy. *Oncology*. 2006;20(10):1157.
5. Li Y, Gao Y, Zhang X, Guo H, Gao H. Nanoparticles in precision medicine for ovarian cancer: From chemotherapy to immunotherapy. *Int J Pharm*. 2020;591:119986.
6. Jayson GC, Kohn EC, Kitchener HC, Ledermann JA. Ovarian cancer. *Lancet*. 2014;384(9951):1376–1388.

7. Ortiz M, Wabel E, Mitchell K, Horibata S. Mechanisms of chemotherapy resistance in ovarian cancer. *Cancer Drug Resist*. 2022;5(2):304.
8. Bauersfeld SP, Kessler CS, Wischnewsky M, et al. The effects of short-term fasting on quality of life and tolerance to chemotherapy in patients with breast and ovarian cancer: a randomized cross-over pilot study. *BMC Cancer*. 2018;18:1–10.
9. Kim D, Nam HJ. PARP inhibitors: clinical limitations and recent attempts to overcome them. *Int J Mol Sci*. 2022;23(15):8412.
10. Amé JC, Spenlehauer C, De Murcia G. The PARP superfamily. *Bioessays*. 2004;26(8):882–893.
11. Wang L, Wang Q, Xu Y, Cui M, Han L. Advances in the treatment of ovarian cancer using PARP inhibitors and the underlying mechanism of resistance. *Current Drug Targets*. 2020;21(2):167–178.
12. Wu Y, Xu S, Cheng S, Yang J, Wang Y. Clinical application of PARP inhibitors in ovarian cancer: from molecular mechanisms to the current status. *Jovarian Res*. 2023;16(1):6.
13. Brown JS, Sundar R, Lopez J. Combining DNA damaging therapeutics with immunotherapy: more haste, less speed. *Br J Cancer*. 2018;118 (3):312–324.
14. Konecny G, Kristeleit R. PARP inhibitors for BRCA1/2-mutated and sporadic ovarian cancer: current practice and future directions. *Br J Cancer*. 2016;115(10):1157–1173.
15. Konstantinopoulos PA, Lheureux S, Moore KN. PARP inhibitors for ovarian cancer: current indications, future combinations, and novel assets in development to target DNA damage repair. *Am Soc Clin Oncol Educat Book*. 2020;40:e116–e131.
16. Tung N, Garber JE. PARP inhibition in breast cancer: progress made and future hopes. *NPJ Breast Cancer*. 2022;8(1):47.
17. Chi J, Chung SY, Parakrama R, Fayyaz F, Jose J, Saif MW. The role of PARP inhibitors in BRCA mutated pancreatic cancer. *Ther Adv Gastroenterol*. 2021;14:17562848211014818.
18. Kim G, Ison G, McKee AE, et al. FDA approval summary: olaparib monotherapy in patients with deleterious germline BRCA-mutated advanced ovarian cancer treated with three or more lines of chemotherapy. *Clin Cancer Res*. 2015;21(19):4257–4261.
19. Franzese E, Centonze S, Diana A, et al. PARP inhibitors in ovarian cancer. *Cancer Treat Rev*. 2019;73:1–9.
20. Xu Q, Li Z. Update on poly ADP-ribose polymerase inhibitors in ovarian cancer with non-BRCA mutations. *Front Pharmacol*. 2021;12:743073.
21. Pathade AD, Kommineni N, Bulbake U, Thummar MM, Samanthula G, Khan W. Preparation and comparison of oral bioavailability for different nano-formulations of olaparib. *AAPS Pharm Sci Tech*. 2019;20:1–13.
22. Alali AS, Kalam MA, Ahmed MM, et al. Nanocrystallization improves the solubilization and cytotoxic effect of a poly (adp-ribose)-polymerase-i inhibitor. *Polymers*. 2022;14(22):4827.
23. Martel R, Klicius J, Galet S. Inhibition of the immune response by rapamycin, a new antifungal antibiotic. *Can J Physiol Pharmacol*. 1977;55 (1):48–51.
24. Guba M, von Breitenbuch P, Steinbauer M, et al. Rapamycin inhibits primary and metastatic tumor growth by antiangiogenesis: involvement of vascular endothelial growth factor. *Nature Med*. 2002;8(2):128–135.
25. Laplante M, Sabatini DM. mTOR signaling in growth control and disease. *cell*. 2012;149(2):274–293.
26. Li J, Kim SG, Blenis J. Rapamycin: one drug, many effects. *Cell Metab*. 2014;19(3):373–379.
27. Easton JB, Houghton PJ. Therapeutic potential of target of rapamycin inhibitors. *Expert Opin Therap Target*. 2004;8(6):551–564.
28. Ito D, Fujimoto K, Mori T, et al. In vivo antitumor effect of the mTOR inhibitor CCI-779 and gemcitabine in xenograft models of human pancreatic cancer. *International Journal of Cancer*. 2006;118(9):2337–2343.
29. Javle MM, Shroff RT, Xiong H, et al. Inhibition of the mammalian target of rapamycin (mTOR) in advanced pancreatic cancer: results of two Phase II studies. *BMC Cancer*. 2010;10:1–7.
30. Li H, Tong J, Cao W, et al. Longitudinal non-vascular transport pathways originating from acupuncture points in extremities visualised in human body. *Chin Sci Bull*. 2014;59:5090–5095.
31. Ghezzi M, Pescina S, Padula C, et al. Polymeric micelles in drug delivery: an insight of the techniques for their characterization and assessment in biorelevant conditions. *J Control Release*. 2021;332:312–336.
32. Perumal S, Atchudan R, Lee W. A review of polymeric micelles and their applications. *Polymers*. 2022;14(12):2510.
33. Xu W, Ling P, Zhang T. Polymeric micelles, a promising drug delivery system to enhance bioavailability of poorly water-soluble drugs. *J Drug Delivery*. 2013;2013:340315.
34. Hwang D, Ramsey JD, Kabanov AV. Polymeric micelles for the delivery of poorly soluble drugs: From nanoformulation to clinical approval. *Adv Drug Delivery Rev*. 2020;156:80–118.
35. Lv S, Wu Y, Cai K, et al. High drug loading and sub-quantitative loading efficiency of polymeric micelles driven by donor–receptor coordination interactions. *J Am Chem Soc*. 2018;140(4):1235–1238.
36. Owen SC, Chan DP, Shoichet MS. Polymeric micelle stability. *Nano Today*. 2012;7(1):53–65.
37. Lu Y, Zhang E, Yang J, Cao Z. Strategies to improve micelle stability for drug delivery. *Nano Res*. 2018;11:4985–4998.
38. Kaur J, Gulati M, Jha NK, et al. Recent advances in developing polymeric micelles for treating cancer: breakthroughs and bottlenecks in their clinical translation. *Drug Discover Today*. 2022;27(5):1495–1512.
39. Zhang Z, Tan S, Feng -S-S. Vitamin E TPGS as a molecular biomaterial for drug delivery. *Biomaterials*. 2012;33(19):4889–4906.
40. Traber MG, Schiano TD, Steephen AC, Kayden HJ, Shike M. Efficacy of water-soluble vitamin E in the treatment of vitamin E malabsorption in short-bowel syndrome. *The Am J Clinl Nut*. 1994;59(6):1270–1274.
41. Neophytou CM, Constantinou C, Papageorgis P, Constantinou AI. D-alpha-tocopheryl polyethylene glycol succinate (TPGS) induces cell cycle arrest and apoptosis selectively in Survivin-overexpressing breast cancer cells. *Biochem Pharmacol*. 2014;89(1):31–42.
42. Fischer JR, Harkin KR, Freeman LC. Concurrent administration of water-soluble vitamin E can increase the oral bioavailability of cyclosporine a in healthy dogs. *Veter Therap*. 2002;3(4):465–473.
43. Mi Y, Liu Y, Feng -S-S. Formulation of docetaxel by folic acid-conjugated D-α-tocopheryl polyethylene glycol succinate 2000 (Vitamin E TPGS2k) micelles for targeted and synergistic chemotherapy. *Biomaterials*. 2011;32(16):4058–4066.
44. Youk H-J, Lee E, Choi M-K, et al. Enhanced anticancer efficacy of α-tocopheryl succinate by conjugation with polyethylene glycol. *J Control Release*. 2005;107(1):43–52.
45. Collnot E-M, Baldes C, Wempe MF, et al. Mechanism of inhibition of P-glycoprotein mediated efflux by vitamin E TPGS: influence on ATPase activity and membrane fluidity. *Mol Pharmaceut*. 2007;4(3):465–474.

46. Liu T, Liu X, Xiong H, et al. Mechanisms of TPGS and its derivatives inhibiting P-glycoprotein efflux pump and application for reversing multidrug resistance in hepatocellular carcinoma. *Polym Chem*. 2018;9(14):1827–1839.
47. Nguyen -T-T-L, Duong V-A, Maeng H-J. Pharmaceutical formulations with P-glycoprotein inhibitory effect as promising approaches for enhancing oral drug absorption and bioavailability. *Pharmaceutics*. 2021;13(7):1103.
48. Callaghan R, Luk F, Bebawy M. Inhibition of the multidrug resistance P-glycoprotein: time for a change of strategy? *Drug Metab Dispos*. 2014;42(4):623–631.
49. Waghray D, Zhang Q. Inhibit or evade multidrug resistance P-glycoprotein in cancer treatment: miniperspective. *J Med Chem*. 2017;61 (12):5108–5121.
50. Zeng Y-C, Li S, Liu C, et al. Soluplus micelles for improving the oral bioavailability of scopoletin and their hypouricemic effect in vivo. *Acta Pharmacol Sin*. 2017;38(3):424–433.
51. Kang N, Perron M-È, RE P, Zhang Y, Gaucher G, Leroux J-C. Stereocomplex block copolymer micelles: core− shell nanostructures with enhanced stability. *Nano Lett*. 2005;5(2):315–319.
52. Lo CL, Lin KM, Huang CK, Hsiue GH. Self-assembly of a micelle structure from graft and diblock copolymers: an example of overcoming the limitations of polyions in drug delivery. *Adv Funct Mater*. 2006;16(18):2309–2316.
53. Saxena V, Hussain MD. Polymeric mixed micelles for delivery of curcumin to multidrug resistant ovarian cancer. *J biomed nanotech*. 2013;9 (7):1146–1154.
54. Cagel M, Tesan FC, Bernabeu E, et al. Polymeric mixed micelles as nanomedicines: achievements and perspectives. *Eur. J. Pharm. Biopharm*. 2017;113:211–228.
55. Wang Y, Ding Y, Xu Y, et al. Mixed micelles of TPGS and Soluplus® for co-delivery of paclitaxel and fenretinide: in vitro and in vivo anticancer study. *Pharm Develop Tech*. 2020;25(7):865–873.
56. Ding Y, Ding Y, Wang Y, et al. Soluplus®/TPGS mixed micelles for co-delivery of docetaxel and piperine for combination cancer therapy. *Pharm Develop Tech*. 2020;25(1):107–115.
57. Thakuri PS, Gupta M, Plaster M, Tavana H. Quantitative size-based analysis of tumor spheroids and responses to therapeutics. *ASSAY Drug Dev Technol*. 2019;17(3):140–149.
58. Han SJ, Kwon S, Kim KS. Challenges of applying multicellular tumor spheroids in preclinical phase. *Can Cell Inter*. 2021;21:1–19.
59. Habanjar O, Diab-Assaf M, Caldefie-Chezet F, Delort L. 3D cell culture systems: tumor application, advantages, and disadvantages. *Int J Mol Sci*. 2021;22(22):12200.
60. Katt ME, Placone AL, Wong AD, Xu ZS, Searson PC. In vitro tumor models: advantages, disadvantages, variables, and selecting the right platform. *Front Bioeng Biotechnol*. 2016;4:12.
61. Park J, Choi Y, Chang H, Um W, Ryu JH, Kwon IC. Alliance with EPR effect: combined strategies to improve the EPR effect in the tumor microenvironment. *Theranostics*. 2019;9(26):8073.
62. Wu J. The enhanced permeability and retention (EPR) effect: the significance of the concept and methods to enhance its application. *J Personalized Med*. 2021;11(8):771.
63. Zhang H. Thin-film hydration followed by extrusion method for liposome preparation. *Liposomes*. 2017;2017:17–22.
64. Das UK, Bordoloi R, Ganguly S. Freeze-drying technique and its wide application in biomedical and pharmaceutical sciences. *Res J Chem Environ Sci*. 2014;2(3):01–04.
65. Van Meerloo J, Kaspers GJ, Cloos J. Cell sensitivity assays: the MTT assay. *Cancer Cell Cult*. 2011;237–245.
66. Ashton JC. Drug combination studies and their synergy quantification using the Chou–Talalay method. *Cancer Res*. 2015;75(11):2400.
67. Cai X, Yang W, Huang L, Zhu Q, Liu S. A series of sensitive and visible fluorescence-turn-on probes for CMC of ionic surfactants: design, synthesis, structure influence on CMC and sensitivity, and fast detection via a plate reader and a UV light. *Sensors and Actuat B Chem*. 2015;219:251–260.
68. Karimi MA, Mozaheb MA, Hatefi-Mehrjardi A, Tavallali H, Attaran AM, Shamsi R. A new simple method for determining the critical micelle concentration of surfactants using surface plasmon resonance of silver nanoparticles. *J Anal Sci Technol*. 2015;6(1):1–8.
69. Modi S, Anderson BD. Determination of drug release kinetics from nanoparticles: overcoming pitfalls of the dynamic dialysis method. *Mol Pharmaceut*. 2013;10(8):3076–3089.
70. Schwartz JB, Simonelli AP, Higuchi WI. Drug release from wax matrices I. Analysis of data with first-order kinetics and with the diffusion-controlled model. *J Pharmaceut Sci*. 1968;57(2):274–277.
71. Zhang L-N, Chen J, Huang X-G, Meng H-Y, Tan C-H. A Study on the Fluorescence Properties of New Laser Material--B 18 H 22 in SDS Aqueous Solution. *Int J Opt*. 2019;2019:5160381.
72. Anand U, Jash C, Mukherjee S. Spectroscopic determination of Critical Micelle Concentration in aqueous and non-aqueous media using a non-invasive method. *J Colloid Interface Sci*. 2011;364(2):400–406.
73. Wu D, Wang Z, Lin M, et al. In vitro and in vivo antitumor activity of cucurbitacin C, a novel natural product from cucumber. *Front Pharmacol*. 2019;10:1287.
74. Z-p L, G-x T, Jiang H, et al. Liver-targeting and pH-sensitive sulfated hyaluronic acid mixed micelles for hepatoma therapy. *Int j Nanomed*. 2019;9437–9452.
75. Shackleton M Normal stem cells and cancer stem cells: similar and different. Paper presented at: Seminars in cancer biology; 2010.
76. Yeldag G, Rice A, Del Río Hernández A. Chemoresistance and the self-maintaining tumor microenvironment. *Cancers*. 2018;10(12):471.
77. Ishiguro T, Ohata H, Sato A, Yamawaki K, Enomoto T, Okamoto K. Tumor-derived spheroids: relevance to cancer stem cells and clinical applications. *Cancer Scie*. 2017;108(3):283–289.
78. Kwak TH, Kang JH, Hali S, et al. Generation of homogeneous midbrain organoids with in vivo-like cellular composition facilitates neurotoxin-based Parkinson's disease modeling. *Stem Cells*. 2020;38(6):727–740.
79. Vinci M, Gowan S, Boxall F, et al. Advances in establishment and analysis of three-dimensional tumor spheroid-based functional assays for target validation and drug evaluation. *BMC Biol*. 2012;10:1–21.
80. Burkholder T, Foltz C, Karlsson E, Linton CG, Smith JM. Health evaluation of experimental laboratory mice. *Current Prot Mouse Biol*. 2012;2 (2):145–165.
81. Foltz CJ, Ullman-Cullere M. Guidelines for assessing the health and condition of mice. *Lab Animal*. 1999;28(5):1999.

82. Toth LA. Defining the moribund condition as an experimental endpoint for animal research. *ILAR j*. 2000;41(2):72–79.
83. Leow CC, Coffman K, Inigo I, et al. MEDI3617, a human anti-angiopoietin 2 monoclonal antibody, inhibits angiogenesis and tumor growth in human tumor xenograft models. *Int j Oncol*. 2012;40(5):1321–1330.
84. Kersemans V, Cornelissen B, Allen PD, Beech JS, Smart SC. Subcutaneous tumor volume measurement in the awake, manually restrained mouse using MRI. *J Magn Reson Imaging*. 2013;37(6):1499–1504.
85. Xu J, Zhu W, Yao X, et al. Mesoporous Organosilica-Based Hydrogen Sulfide Nanogenerator for Enhanced Tumor Chemotherapy. *ACS Appl Nano Mater*. 2023;3:12029.
86. Kim J, Cho Y-J, Ryu J-Y, et al. CDK7 is a reliable prognostic factor and novel therapeutic target in epithelial ovarian cancer. *Gynecologic Oncol*. 2020;156(1):211–221.
87. Zhang RX, Wong HL, Xue HY, Eoh JY, Wu XY. Nanomedicine of synergistic drug combinations for cancer therapy–Strategies and perspectives. *J Control Release*. 2016;240:489–503.
88. Pathi S, Chennuru R, Bollineni M Olaparib Co-Crystals and Process of Preparation Thereof. *WIPO (PCT) Patent No. WO2021044437A1*; 2021;3.
89. Perinelli DR, Cespi M, Lorusso N, Palmieri GF, Bonacucina G, Blasi P. Surfactant self-assembling and critical micelle concentration: one approach fits all? *Langmuir*. 2020;36(21):5745–5753.
90. Jiang B-H, Tseng W-L, H-Y L, et al. Poly (ADP-ribose) polymerase 1: cellular pluripotency, reprogramming, and tumorogenesis. *Int J Mol Sci*. 2015;16(7):15531–15545.
91. Hay N, Sonenberg N. Upstream and downstream of mTOR. *Genes Dev*. 2004;18(16):1926–1945.
92. Bazzo GC, Pezzini BR, Stulzer HK. Eutectic mixtures as an approach to enhance solubility, dissolution rate and oral bioavailability of poorly water-soluble drugs. *Int J Pharm*. 2020;588:119741.
93. Feng S, Zhang Z, Almotairy A, Repka MA. Development and evaluation of polymeric mixed micelles prepared using Hot-melt extrusion for extended delivery of poorly water-soluble drugs. *J Pharmaceut Sci*. 2023:112:2869.
94. Srivastava A, Uchiyama H, Wada Y, et al. Mixed micelles of the antihistaminic cationic drug diphenhydramine hydrochloride with anionic and non-ionic surfactants show improved solubility, drug release and cytotoxicity of ethenzamide. *J Mol Liq*. 2019;277:349–359.
95. Fang J, Islam W, Maeda H. Exploiting the dynamics of the EPR effect and strategies to improve the therapeutic effects of nanomedicines by using EPR effect enhancers. *Adv Drug Delivery Rev*. 2020;157:142–160.
96. Torchilin V. Tumor delivery of macromolecular drugs based on the EPR effect. *Adv Drug Delivery Rev*. 2011;63(3):131–135.
97. Chen G, Li D, Jin Y, et al. Deformable liposomes by reverse-phase evaporation method for an enhanced skin delivery of (+)-catechin. *Drug Dev Ind Pharm*. 2014;40(2):260–265.
98. Sunoqrot S, Aliyeh S, Abusulieh S, Sabbah D. Vitamin E TPGS-poloxamer nanoparticles entrapping a novel PI3Kα inhibitor potentiate its activity against breast cancer cell lines. *Pharmaceutics*. 2022;14(9):1977.
99. Li Y, Tan X, Liu X, et al. Enhanced anticancer effect of doxorubicin by TPGS-coated liposomes with Bcl-2 siRNA-Corona for dual suppression of drug resistance. *Asian J. Pharm. Sci*. 2020;15(5):646–660.
100. Liu H, Tu L, Zhou Y, et al. Improved bioavailability and antitumor effect of docetaxel by TPGS modified proniosomes: in vitro and in vivo evaluations. *Sci Rep*. 2017;7(1):43372.
101. Chen Y, Mo L, Wang X, et al. TPGS-1000 exhibits potent anticancer activity for hepatocellular carcinoma in vitro and in vivo. *Aging*. 2020;12 (2):1624.
102. Su H, Wang F, Ran W, et al. The role of critical micellization concentration in efficacy and toxicity of supramolecular polymers. *Proceedings of the National Academy of Sciences*. 2020;117(9):4518–4526.
103. Patra A, Satpathy S, Shenoy AK, Bush JA, Kazi M, Hussain MD. Formulation and evaluation of mixed polymeric micelles of quercetin for treatment of breast, ovarian, and multidrug resistant cancers. *Int j Nanomed*. 2018;2018:2869.
104. Bernabeu E, Gonzalez L, Cagel M, Gergic EP, Moretton MA, Chiappetta DA. Novel Soluplus®—TPGS mixed micelles for encapsulation of paclitaxel with enhanced in vitro cytotoxicity on breast and ovarian cancer cell lines. *Colloids Surf B*. 2016;140:403–411.
105. Cagel M, Bernabeu E, Gonzalez L, et al. Mixed micelles for encapsulation of doxorubicin with enhanced in vitro cytotoxicity on breast and ovarian cancer cell lines versus Doxil®. *Biomed Pharm*. 2017;95:894–903.
106. Mansoori B, Mohammadi A, Davudian S, Shirjang S, Baradaran B. The different mechanisms of cancer drug resistance: a brief review. *Adv Pharm Bull*. 2017;7(3):339.
107. Karthika C, Sureshkumar R, Zehravi M, et al. Multidrug resistance in cancer cells: focus on a possible strategy plan to address colon carcinoma cells. *Life*. 2022;12(6):811.
108. Behzadi S, Serpooshan V, Tao W, et al. Cellular uptake of nanoparticles: journey inside the cell. *Chem Soc. Rev*. 2017;46(14):4218–4244.
109. Hu X, Han R, Quan L-H, Liu C-Y, Liao Y-H. Stabilization and sustained release of zeylenone, a soft cytotoxic drug, within polymeric micelles for local antitumor drug delivery. *Int J Pharm*. 2013;450(1–2):331–337.
110. Mueller-Goymann C, Hamann H-J. Sustained release from reverse micellar solutions by phase transformations into lamellar liquid crystals. *J Control Release*. 1993;23(2):165–174.
111. Chen L, Sha X, Jiang X, Chen Y, Ren Q, Fang X. Pluronic P105/F127 mixed micelles for the delivery of docetaxel against Taxol-resistant non-small cell lung cancer: optimization and in vitro, in vivo evaluation. *Int j Nanomed*. 2013;73–84.
112. Wan X, Beaudoin JJ, Vinod N, et al. Co-delivery of paclitaxel and cisplatin in poly (2-oxazoline) polymeric micelles: Implications for drug loading, release, pharmacokinetics and outcome of ovarian and breast cancer treatments. *Biomaterials*. 2019;192:1–14.
113. Senapati S, Mahanta AK, Kumar S, Maiti P. Controlled drug delivery vehicles for cancer treatment and their performance. *Signal Transduct Target Ther*. 2018;3(1):7.
114. Huang X, Brazel CS. On the importance and mechanisms of burst release in matrix-controlled drug delivery systems. *J Control Rel*. 2001;73(2–3):121–136.
115. Khan A, Marques EF. Synergism and polymorphism in mixed surfactant systems. *Curr Opin Colloid Interface Sci*. 1999;4(6):402–410.
116. Lu Y, Yue Z, Xie J, et al. Micelles with ultralow critical micelle concentration as carriers for drug delivery. *Nat Biomed Eng*. 2018;2 (5):318–325.

117. Kim H-U, Lim K-H. Description of temperature dependence of critical micelle concentration. *Bullet Korean Chem Socie*. 2003;24(10):1449–1454.
118. Constantinides PP, Han J, Davis SS. Advances in the use of tocols as drug delivery vehicles. *Pharm Res*. 2006;23:243–255.
119. Jin IS, Jo MJ, Park C-W, Chung YB, Kim J-S, Shin DH. Physicochemical, pharmacokinetic, and toxicity evaluation of soluplus® polymeric micelles encapsulating fenbendazole. *Pharmaceutics*. 2020;12(10):1000.
120. Talbot SR, Biernot S, Bleich A, et al. Defining body-weight reduction as a humane endpoint: a critical appraisal. *Laboratory Animals*. 2020;54(1):99–110.
121. Kapałczyńska M, Kolenda T, Przybyła W, et al. 2D and 3D cell cultures–a comparison of different types of cancer cell cultures. *Arch Med Sci*. 2018;14(4):910–919.
122. Aryal S, Hu C-MJ, Zhang L. Polymeric nanoparticles with precise ratiometric control over drug loading for combination therapy. *Mol Pharmaceut*. 2011;8(4):1401–1407.
123. Guo Y, Li X, Macgregor RB, Yan H, Zhang RX. Microfluidics-based PLGA nanoparticles of ratiometric multidrug: From encapsulation and release rates to cytotoxicity in human lens epithelial cells. *Heliyon*. 2023;9(7).
124. Zhao H, Yung LYL. Addition of TPGS to folate-conjugated polymer micelles for selective tumor targeting. *J Biomed Mater Res Part A*. 2009;91(2):505–518.
125. Hao T, Chen D, Liu K, et al. Micelles of d-α-tocopheryl polyethylene glycol 2000 succinate (TPGS 2K) for doxorubicin delivery with reversal of multidrug resistance. *ACS Appl Mater Interfaces*. 2015;7(32):18064–18075.
126. Bhendale M, Singh JK. Molecular insights on morphology, composition, and stability of mixed micelles formed by ionic surfactant and nonionic block copolymer in water using coarse-grained molecular dynamics simulations. *Langmuir*. 2023;39(14):5031–5040.
127. Chaudhary A, Rajiv T, Dagur P, Suddhasattya D, Ghosh M. Stability indicating assay method for the quantitative determination of Olaparib in bulk and pharmaceutical dosage form. *Turkish J Pharm Scien*. 2022;19(5):488.
128. Wu Y, Dong G, Sheng C. Targeting necroptosis in anticancer therapy: mechanisms and modulators. *Acta Pharmaceutica Sinica B*. 2020;10(9):1601–1618.
129. Chen G, Gong R, Shi X, et al. Halofuginone and artemisinin synergistically arrest cancer cells at the G1/G0 phase by upregulating p21Cip1 and p27Kip1. *Oncotarget*. 2016;7(31):50302.